Equivalent linear model for the lateral dynamic analysis of pile foundations considering pile-soil interface degradation*

Francisco González†, Luis A. Padrón, Juan J. Aznárez, and Orlando Maeso

University Institute of Intelligent Systems and Numerical Applications in Engineering (SIANI), Universidad de Las Palmas de Gran Canaria, Spain

Abstract

An equivalent linear BEM-FEM model for the approximate analysis of the time harmonic lateral response of piles considering soil degradation along the soil-pile interface is proposed. The non-degraded soil around the foundation is modelled with boundary elements as a continuum, semi-infinite, isotropic, homogeneous or zoned homogeneous, linear, viscoelastic medium. Piles are modelled with finite elements as beams according to the Bernoulli hypothesis. Differently from what is considered in other BEM-FEM coupled numerical schemes, welded contact conditions are not assumed herein between piles and soil. On the contrary, displacements along FEM piles and within BEM soil are related through distributed springs and dashpots whose properties vary along the pile and that represent the varying stiffness and energy dissipation properties of a pile-soil interface with different levels of degradation at different depths. The developed numerical model is verified by comparison against a more rigorous but much more costly multi-domain boundary element model in which the same degraded soil regions around the pile are modelled as three-dimensional regions.

Keywords: pile foundations; pile-soil interaction; soil degradation; BEM-FEM coupling; dynamic impedances.

1 Introduction

When piles are subjected to significant dynamic loads, such as those caused by machine vibration, wind over the superstructure, or seismic actions, high levels of stress and strain are likely to develop along the pile-soil interface (more probably in the upper parts of the pile) and induce effects such as soil degradation in the soil region immediately adjacent to the pile. Separation (gapping) can also occur close to the soil surface due to the low confinement pressure. These phenomena lead to damaged or imperfect pile-soil interfaces that should be taken into account in the process of design of pile foundations and piled structures subjected to dynamic loads.

*This is the peer reviewed version of the following article: F. González, L. A. Padrón, J. J. Aznárez, O. Maeso, Equivalent linear model for the lateral dynamic analysis of pile foundations considering pile-soil interface degradation, *Engineering Analysis with Boundary Elements*, 119:59-73, 2020, which has been published in final form at https://doi.org/10.1016/j.enganabound.2020.07.006. This article may be used for non-commercial purposes in accordance with Elsevier Terms and Conditions for Accepted Manuscripts.

†Corresponding author: Francisco González, Instituto Universitario de Sistemas Inteligentes y Aplicaciones Numéricas en Ingeniería, Universidad de Las Palmas de Gran Canaria, Edificio Central del Parque Científico y Tecnológico del Campus Universitario de Tafira, 35017 Las Palmas de Gran Canaria, Spain.
E-mail: `francisco.gonzalez@ulpgc.es`

The dynamic and seismic response of piles under linear-elastic assumptions constitutes a topic that has received significant attention. The time-harmonic dynamic response of pile foundations, whose knowledge allows the use of sub-structuring approaches for the analysis of piled structures, has been studied through a number of approaches: a) analytical approaches that are rigorous but limited to a specific problem, lacking versatility and generality (see e.g. [1, 2, 3]); b) simplified semi-analytical procedures, including Winkler-type models, that are focused on the computation of the foundation impedance functions (see e.g. [4, 5, 6]), or on the analysis of the kinematic interaction (see e.g. [7, 8, 9]; and c) numerical techniques such as the Finite Element Method (FEM) (see e.g. [10, 11, 12]) that can be very versatile but having difficulties in modelling unbounded regions as the soil; the Boundary Element Method (BEM) (see e.g. [13, 14, 15]) by assuming Green's functions for the soil behaviour which only require meshing the boundaries and interfaces of the problem; or coupled BEM-FEM schemes taking the advantages of both methodologies: BEM formulations for the soil and structural monodimensional FEM elements for the piles. This last approach has been very appealing since the early 80's (see e.g. [16, 17, 18, 19, 20]). Also nowadays, this strategy is taken into account in models developed for a further understanding of the dynamic behaviour of pile foundations, either by using the full-space fundamental solution in the frequency domain (see e.g. [21]) or fundamental solutions for the layered half-space in the frequency domain (see e.g. [22]) or in the time domain (see e.g. [23]).

The dynamic response of pile foundations taking different types of nonlinearities into account has also received a significant amount of attention. Experimental studies that have provided relevant data for advancing in the knowledge of these phenomena and have, therefore, contributed in the development of new numerical models cover full-scale systems, e.g. [24, 25, 26], scaled 1g experimental models, e.g. [27, 28, 29], and centrifuge tests, e.g. [30, 31, 32]. Developed numerical models in this regard include Beam on Nonlinear Winkler Foundation (BNWF) approaches, finite element formulations, and models that consider a weak zone in the soil around the pile. It has been a hard task for researchers to propose reliable and complete models that account for different types of dynamic nonlinearities involved in the problem.

BNWF models are popular due to the possibility of implementing all kinds of geometrical and material behaviour laws with limited complexity, which makes them versatile and computationally not very costly (see e.g. [33, 34, 35, 36]). However, modelling the soil medium through a series of one-dimensional springs, usually uncoupled among them, constitutes an approach with limitations when it comes to taking into account the three-dimensionality of the problem, and specially in stratified or anisotropic soils. At the same time, the characterization of the laws of the nonlinear springs is not a trivial task, and involves a significant amount of uncertainty. For instance, Rhamani et al. [37] found recently that BNWF models fail to predict accurately the response of soil-pile systems under dynamic or seismic loads even if they incorporate API p-y curves or more specific p-y curves derived from continuum models. Consequently, they recommended the use continuum models.

Gerolymos et al. [38] found a good agreement between results of a BNWF model and those of a nonlinear finite element model for the dynamic analysis of piles including soil and interface nonlinearities. In fact, models based on finite element formulations are also very popular (see e.g. [39, 40, 41]). They can be advanced, and can incorporate a significant amount of detail and complexity, but are therefore complicated to set up and verify properly, and can be computationally expensive. A significant source of uncertainty lies in the calibration of the different parameters involved, specially those related to the nonlinear constitutive laws. Mesh and boundary conditions imposed at the edges where the soil mesh is truncated, are additional sources of uncertainty.

A different approach is based on approximately incorporate to the model the effects of degradation and lack of bond by including a cylindrical soil zone around the pile whose shear modulus and material damping differ from those of the outer medium [42, 43, 44, 45].

In fact, linear equivalent models can be very appealing if they are able to incorporate the most significant features influencing the dynamic response of the soil-pile system. They are computa-

tionally very efficient and can be used in substructuring analysis, in optimization algorithms and in parametric studies. However, traditional equivalent linear soil models could underestimate the structural acceleration response under seismic action, as stated recently by Luo et al. [46].

Thus, this work aims at proposing a new equivalent linear numerical model for the approximate analysis of pile-soil systems with degraded or damaged pile-soil interfaces. The model assumes that the soil immediately adjacent to the pile shaft develops a certain level of degradation, which is usually a function of depth. It is well-known that soils that have undergone high levels of strain, experience a process of reduction of its shear modulus and an increase of its material damping ratio (see e.g. [47, 48, 49]). This is depicted in Figure 1, where the representative shape of the curves of evolution of shear modulus and damping ratio with shear strain are shown. Depending on the stiffness and type of soil (sand, normal- or over-consolidated clay), and also on the depth of the water table or soil properties such as the plasticity index, the variation in the soil shear modulus and material damping ratio as a function of shear strain is different. Eurocode–8 [50], within its fifth part, Section 4.2.3, states that, in such cases, the differences between small-strain values of the shear wave velocity and those compatible with the strain levels induced by the design earthquake should be taken into account, and provides indications on damping ratios and shear modulus reduction factors as a function of ground acceleration ratio.

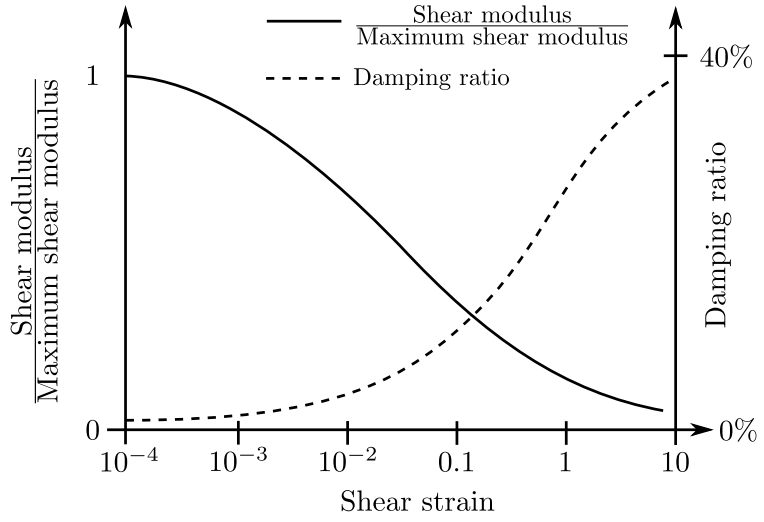

Figure 1: Generic depiction of the variation of the soil shear modulus and the soil damping ratio as a function of soil shear strain.

The proposal is based on a coupled BEM-FEM approach, uniting the advantages of both methods: the piles are modelled as beam with finite elements; the degraded or imperfect pile-soil interface is represented by distributed springs and dashpots whose properties vary with depth; and the soil beyond the degraded interface is modelled by boundary elements.

The starting point of this model is another previous one developed by some of the authors (Padrón et al. [21]). That model is based on the idea of a previous static approach (Mendonça and Paiva [51]) where it is assumed that the continuity of the soil is not altered by the presence of the piles and where the tractions in the pile-soil interface are considered as a load-line applied within the half-space in the boundary integral representation of the soil. It allows to simplify the formulation of the model without significant loss of accuracy in the problems treated. The starting formulation can rigorously take into account layered soils [52], pile groups [53] and inclined piles [54].

The perfectly bonded compatibility conditions between pile and soil assumed in the starting formulation [21] is generalized in the present proposal to soil-pile equilibrium equations accounting for contact effects through the inclusion of the mentioned distributed springs and dashpots between pile and soil load-line. Parameters that define the distributed springs and dashpots along the pile-soil

interface can later be calibrated against numerical and empirical results, and can be used in efficient parametric analysis by substructuring or direct methodologies in the frequency domain.

This paper focuses on the model description for the lateral dynamic analysis of pile foundations considering pile-soil interface degradation and also its validation. To this end, the developed numerical tool is defined in Section 2, and the reference and more rigorous tool used for comparison purposes is defined in Section 3.1. Calibration results are presented in Sections 3.2 in terms of horizontal impedance functions of single pile foundations. Then, the inclusion of the degradation damping, which has been shown to be an essential phenomena involved in the system, is validated in Section 3.3. Also, varying soil degradation through the pile depth is analysed and validated in terms of horizontal impedance functions in Section 3.4.1, and in terms of displacements along the pile length in Section 3.4.2. The new formulation is computationally more efficient and flexible, easing the study of more complex problems. It and can be extended to study pile groups and generalized to rake piles. On the other hand, the possibility for incorporating more genuine and complex models of soil degradation is completely open.

2 Problem definition and description of the proposed model

The problem under consideration is depicted in Figure 2. A pile is embedded in a homogeneous soil, and is subjected to time harmonic loads (horizontal, vertical or rocking) applied at the pile head. The pile, of length L and diameter d, is assumed to respond as a linear elastic beam with Young's modulus E_p, area and mass moment of inertial A_p and I_p, and material density ρ_p, and will be modelled with Euler-Bernoulli beam finite elements. The mass moments of inertia with respect to both principal axes of inertia of the pile section have been assumed to be identical. Zero material damping is considered for the pile. The non-degraded soil around the foundation is assumed to respond as a horizontally layered isotropic homogeneous viscoelastic medium with Young's modulus E_{s_i} and density ρ_{s_i}, and will be modelled with boundary elements. The material damping of the soil medium is considered by assuming frequency-independent hysteretic damping through complex valued soil modulus of the type $E_{s_i} = \mathrm{Re}[E_{s_i}](1 + 2\mathrm{i}\xi_{s_i})$, where ξ_{s_i} is the damping coefficient in layer i.

Most models of this kind assume perfectly bonded contact conditions between pile and soil, which would imply imposing compatibility conditions between pile and soil displacements. The model proposed herein for the computation of the dynamic response of piles, on the contrary, seeks to take into account, through an equivalent linear approach, the influence of a damaged pile-soil interface representing soil degradation around the pile, together with possible contact effects such as lack of bond. This imperfect pile-soil interface can be visualized as a degraded soil domain surrounding the piles whose mechanical properties differ from those of the undisturbed soil beyond. Besides, damage at the pile-soil interface will usually be a function of depth, as the largest displacements will usually be experienced near the pile head, coinciding with the lowest soil confinement pressures. For this reason, the diameter $d_{\mathrm{dz}}(x_3)$ and shear modulus $G_{\mathrm{dz}}(x_3)$ of such degraded domain are assumed to be also a function of depth. The size of this domain in relation to the pile diameter will be denoted by the dimensionless parameter $\chi(x_3) = d_{\mathrm{dz}}(x_3)/d$.

As depicted in Figure 3, such damaged pile-soil interface is modelled by relating displacements along FEM piles and within BEM soil through distributed springs and dashpots whose properties vary along the pile and that represent the varying stiffness and energy dissipation properties of the pile-soil interface with different levels of degradation at different depths.

The model proposed herein represents a significant evolution of that presented by Padrón et al. [21] in the way in which the compatibility between pile and soil is defined. A brief summary of the discretization scheme adopted for pile and soil load-line is presented in Section 2.1, while a brief summary of the boundary element equations used to describe the dynamic response of the non-degraded soil is presented in Section 2.2, being these aspects of the formulation inherited from

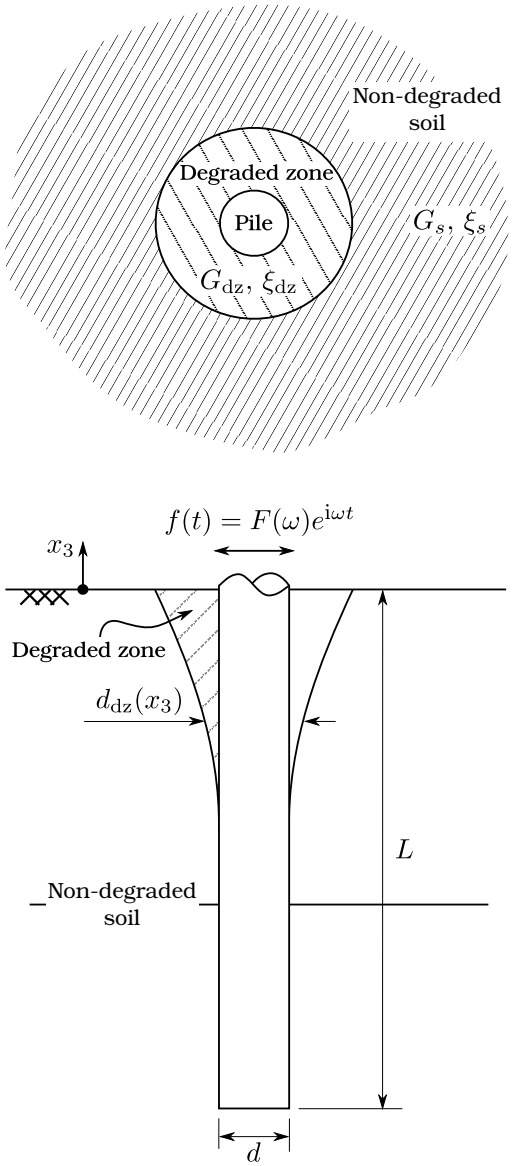

Figure 2: Depiction of the problem.

the starting model as described in [21]. On the other hand, the updated equations of motion and the finite element equations used to describe the dynamic response of the pile are presented in Section 2.3. The major novelties of the proposed formulation are concentrated in Section 2.4, where the pile-soil interface degradation modelling is presented together with the way in which it is included in a BEM-FEM type of model. Finally, in Section 2.5, all involved equations are assembled into a global system matrix of equations.

2.1 Pile and soil load-line discretization

Piles are discretized using three-nodded Euler-Bernoulli beam finite elements with axial deformation, with thirteen degrees of freedom defined in each element: one vertical and two lateral displacements at each node, and two rotations at each one of the extreme nodes, one around each lateral axis of the pile (i.e., torsion excluded). Figure 4 depicts the element, axes and the symbols used to refer to each one of the variables involved. ξ is the elemental dimensionless coordinate varying from $\xi = -1$ to

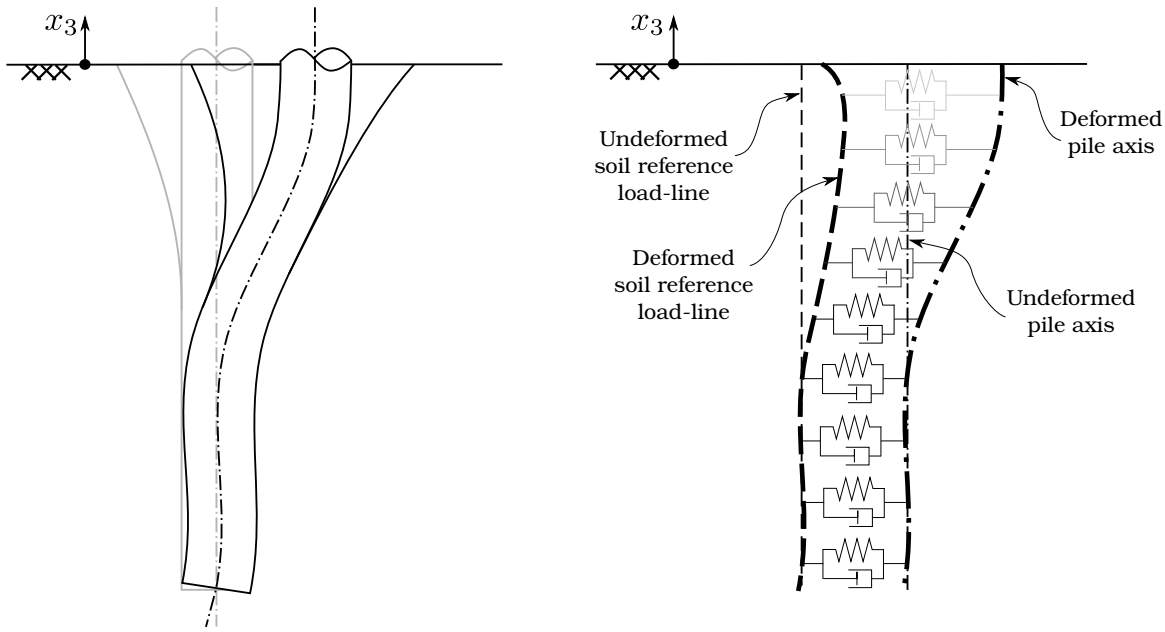

Figure 3: Linear equivalent modelling of an imperfect pile-soil interface through distributed springs and dashpots.

$\xi = 1$. The lateral displacements u_1^p and u_2^p along the pile element are approximated by a set of fourth degree shape functions, while vertical displacements u_3^p are approximated by the three Lagrangian polynomials of second order, so that one can write

$$u_i^p(\xi) = \varphi_1 u_{k_i}^p + \varphi_2 \theta_{k_i}^p + \varphi_3 u_{l_i}^p + \varphi_4 u_{m_i}^p + \varphi_5 \theta_{m_i}^p \,; \quad i = 1, 2 \tag{1a}$$

$$u_3^p(\xi) = \phi_1 u_{k_3}^p + \phi_2 u_{l_3}^p + \phi_3 u_{m_3}^p \tag{1b}$$

where

$$\varphi_1(\xi) = \xi(-\frac{3}{4} + \xi + \frac{1}{4}\xi^2 - \frac{1}{2}\xi^3) \tag{2a}$$

$$\varphi_2(\xi) = \frac{L_e}{8}\xi(-1 + \xi + \xi^2 - \xi^3) \tag{2b}$$

$$\varphi_3(\xi) = 1 - 2\xi^2 + \xi^4 \tag{2c}$$

$$\varphi_4(\xi) = \xi(\frac{3}{4} + \xi - \frac{1}{4}\xi^2 - \frac{1}{2}\xi^3) \tag{2d}$$

$$\varphi_5(\xi) = \frac{L_e}{8}\xi(-1 - \xi + \xi^2 + \xi^3) \tag{2e}$$

and

$$\phi_1(\xi) = \frac{1}{2}\xi(\xi - 1) \tag{3a}$$

$$\phi_2(\xi) = 1 - \xi^2 \tag{3b}$$

$$\phi_3(\xi) = \frac{1}{2}\xi(\xi + 1) \tag{3c}$$

This last set of functions is also used to interpolate within each element the pile-soil contact interaction forces $\mathbf{q}^p$ acting over the pile as

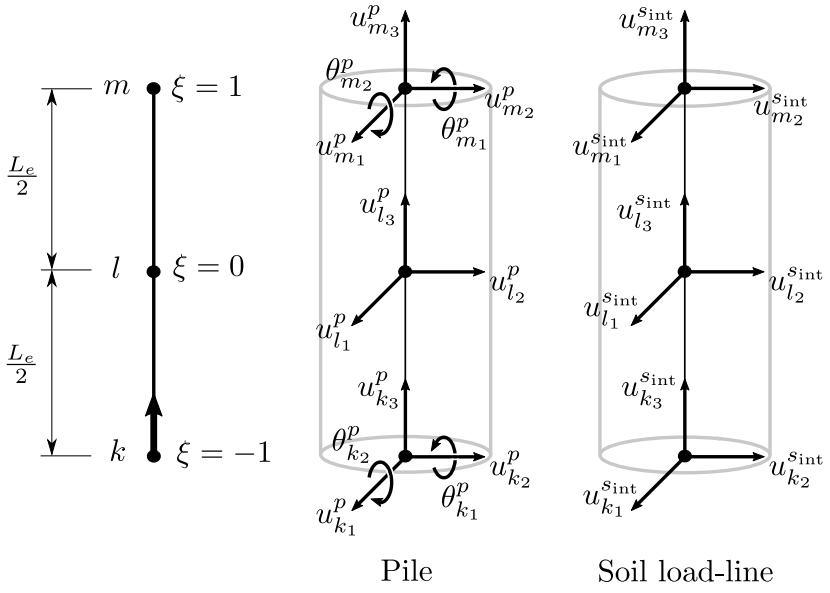

Figure 4: Discretization of pile and soil load-lines.

$$q_i^p(\xi) = \phi_1 q_{k_i}^p + \phi_2 q_{l_i}^p + \phi_3 q_{m_i}^p\,; \quad i = 1,2,3 \tag{4}$$

Similarly, the displacements along the load-lines within the soil are interpolated, also within the element defined before, through an equivalent scheme

$$u_i^{s_{\text{int}}} = \phi_1 u_{k_i}^{s_{\text{int}}} + \phi_2 u_{l_i}^{s_{\text{int}}} + \phi_3 u_{m_i}^{s_{\text{int}}}\,; \quad i = 1,2,3 \tag{5}$$

where $u_{(\cdot)_i}^{s_{\text{int}}}$ are the unknown displacements at internal soil BEM points coinciding with the beam finite element nodes (see Figure 4).

2.2 Boundary element equations

As mentioned before, each stratum of the layered non-degraded soil domain is modelled by BEM. The boundary integral equation for a time-harmonic elastodynamic state defined in a domain Ω_m with boundary Γ^m can be written in a condensed and general form as

$$\mathbf{c}^\iota \mathbf{u}^\iota + \int_{\Gamma^m} \mathbf{p}^* \mathbf{u}\, \mathrm{d}\Gamma = \int_{\Gamma^m} \mathbf{u}^* \mathbf{p}\, \mathrm{d}\Gamma + \int_{\Omega_m} \mathbf{u}^* \mathbf{X}\, \mathrm{d}\Gamma \tag{6}$$

where $\mathbf{c}^\iota$ is the local free term matrix at collocation point $\mathbf{x}^\iota$, $\mathbf{X}$ are the body forces in the domain Ω_m, $\mathbf{u}$ and $\mathbf{p}$ are the displacement and traction over the boundaries, and $\mathbf{u}^*$ and $\mathbf{p}^*$ are the elastodynamic fundamental solution tensors corresponding to the complete space (Cruse and Rizzo [55]).

From the point of view of this formulation for the dynamic behaviour of the soil medium, it is assumed that the soil continuity is not altered by the presence of the piles or by the degraded zone around them. In turn, the effects of the pile-soil interaction are introduced through internal distributed forces located along a so-called load-line within the soil medium. This distributed forces, that will depend on the relationship mentioned above between displacements along the pile and within the soil medium, are treated as body forces, and being the sole body forces involved in the problem, Equation (6) can be written as

$$\mathbf{c}^\iota \mathbf{u}^\iota + \int_{\Gamma^m} \mathbf{p}^* \mathbf{u}\, \mathrm{d}\Gamma = \int_{\Gamma^m} \mathbf{u}^* \mathbf{p}\, \mathrm{d}\Gamma + \int_{\Gamma_l^m} \mathbf{u}^* \mathbf{q}_s\, \mathrm{d}\Gamma_l \tag{7}$$

where Γ_l^m is the soil load-line within the domain Ω_m and $\mathbf{q}_s$ are the pile-soil contact interaction forces induced within the soil domain (see Figure 5a).

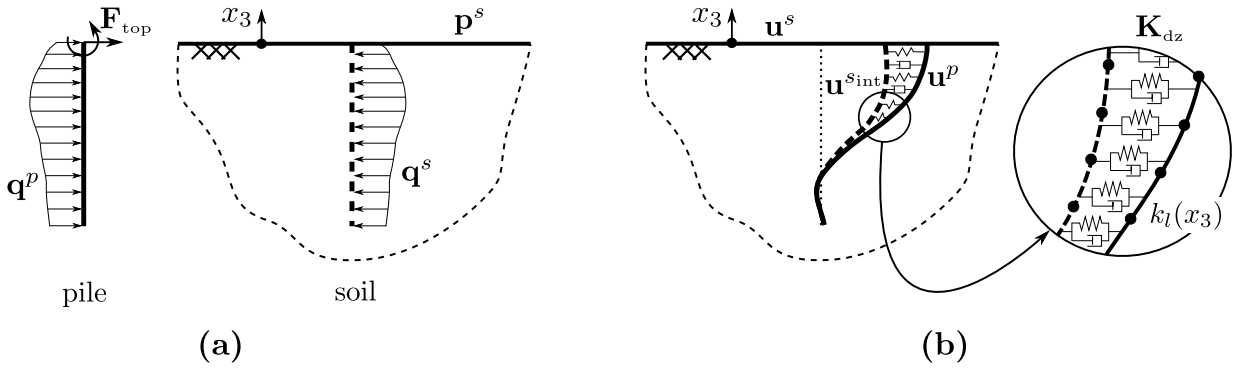

Figure 5: Equilibrium conditions between pile and soil load-line.

These tractions along the soil load-line will also be interpolated in terms of the nodal pile-soil contact interaction forces $\mathbf{q}^s$ defined at internal points coinciding with the nodes of the beam pile finite elements defined before as

$$q_i^s(\xi) = \phi_1 q_{k_i}^s + \phi_2 q_{l_i}^s + \phi_3 q_{m_i}^s\,; \quad i = 1, 2, 3 \tag{8}$$

As shown in Figure 6, the boundaries Γ^m are discretized into quadratic elements of triangular and quadrilateral shapes with six and nine nodes, respectively. Once all boundaries have been discretized, for each region Ω_m, Equation (7) can be written in all nodes on Γ^m in order to obtain a matrix equation of the type

$$\mathbf{H}^{ss}\mathbf{u}^s - \mathbf{G}^{sl}\mathbf{q}^s = \mathbf{G}^{ss}\mathbf{p}^s \tag{9}$$

where $\mathbf{u}^s$ and $\mathbf{p}^s$ are, respectively, the vectors of nodal displacements and tractions on the boundary elements, $\mathbf{H}^{ss}$ and $\mathbf{G}^{ss}$ are coefficient matrices obtained by integration over the boundary elements of the fundamental solution times the corresponding shape functions, and $\mathbf{G}^{sl}$ is the coefficient matrix obtained by numerical integration over the soil load-line of the fundamental solution times the interpolation functions shown in Equation (3), when the unit load is applied on Γ^m.

Furthermore, Equation (7) must be also applied on the internal nodes of the soil load-line leading to

$$\mathbf{H}^{ls}\mathbf{u}^s - \mathbf{G}^{ll}\mathbf{q}^s + \mathbf{C}\mathbf{u}^{s_{\text{int}}} = \mathbf{G}^{ls}\mathbf{p}^s \tag{10}$$

where $\mathbf{H}^{ls}$ and $\mathbf{G}^{ls}$ are coefficient matrices obtained by numerical integration over the boundary elements of the fundamental solution times the corresponding shape functions, $\mathbf{G}^{ll}$ is the coefficient matrix obtained by numerical integration over the soil load-line of the fundamental solution times the interpolation functions shown in Equation (3) when the unit load is applied on the soil load-line, and $\mathbf{u}^{s_{\text{int}}}$ is the vector of nodal displacements along the soil load-line, which is multiplied by the diagonal matrix $\mathbf{C}$, whose non-zero terms are valued 1/2 in positions corresponding to pile nodes placed on a smooth surface, as e.g. pile heads, and unity at the internal points.

2.3 Finite element equations

The time-harmonic dynamic response of the piles, discretized using the linear elastic beam finite elements described in Section 2.1, can be described, in the finite element sense, by the matrix equation

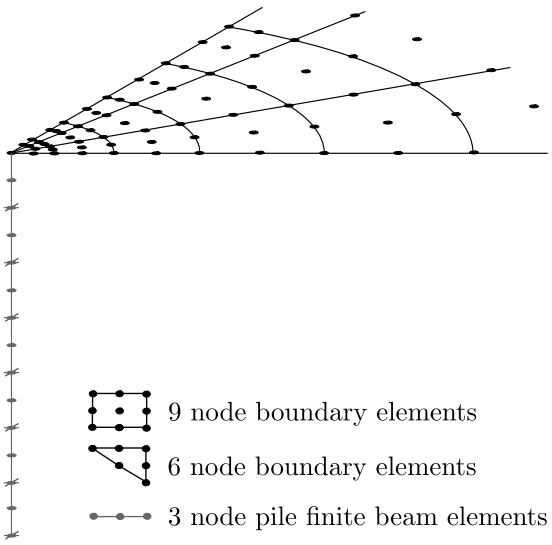

Figure 6: Example of mesh typology used in the model (only a quarter of the geometry is shown).

$$(\mathbf{K}^p - \omega^2\mathbf{M}^p)\mathbf{u}^p - (\mathbf{K}^s - \omega^2\mathbf{M}^s)\mathbf{u}^{s_{\text{int}}} = \mathbf{F}_{\text{top}} + \mathbf{Q}\mathbf{q}^p \tag{11}$$

where $\mathbf{M}^p$ and $\mathbf{K}^p$ are the global mass and stiffness global matrices of the pile, $\mathbf{u}^p$ is the vector of nodal displacements along the pile, $\mathbf{F}_{\text{top}}$ are the forces at the top of the pile, $\mathbf{Q}$ is the global matrix that transforms tractions along the pile to equivalent nodal forces and moments, and ω is the circular frequency of the excitation. The definitions of $\mathbf{M}^p$, $\mathbf{K}^p$ and $\mathbf{Q}$ can be found in [21, 56].

In the case of models where welded contact conditions between pile and soil are assumed, the equation of motion presented in Equation (11) does not include the second term in brackets multiplied by the vector of nodal displacements along the soil load-line $\mathbf{u}^{s_{\text{int}}}$, where $\mathbf{M}^s$ and $\mathbf{K}^s$ are the global mass and stiffness matrices of the soil column occupied by the pile shaft. Thus, this second part of Equation (11) was not present in the simpler model described in [21] and that serves as starting point.

The soil continuity, from the point of view of the BEM model for the soil, is not altered by the presence of the pile. This fact entails that the model would initially overestimate the inertia and stiffness of the pile by taking also into account those of the mentioned soil column. This effect is well known and, given that the inertial effect is very significant, and much more important than the effect of the additional stiffness, it has usually been corrected by subtracting the material soil density from the pile density (see for instance [18, 16, 1, 21]).

On the other hand, displacements along pile and soil load-line are, in the present model, related but not rigidly linked, which prevents from following the simpler strategy mentioned in the previous paragraph and forces to subtract those additional inertia and stiffness proportionally to the displacements of the soil, and not to the displacements of the pile.

These two aspects justify the introduction of the $-(\mathbf{K}^s - \omega^2\mathbf{M}^s)\mathbf{u}^{s_{\text{int}}}$ term, where the mass and stiffness matrices of the soil column have been computed assuming the shear beam model.

Taking into account the discretization described above, and the corresponding shape functions, the element stiffness sub-matrices corresponding to the lateral and axial behaviour (denoted by l and a, respectively) can be obtained as

$$k_{ij}^{s_l} = \int_{L_e} \varphi_i' \cdot G_s A_p \cdot \phi_j' \, \mathrm{d}x_3 \,; \quad \begin{array}{l} i = 1, 2, 3, 4, 5 \,; \\ j = 1, 2, 3 \end{array} \tag{12}$$

and

$$k_{ij}^{s_a} = \int_{L_e} \phi_i' \cdot E_s A_p \cdot \phi_j' \, \mathrm{d}x_3 \, ; \quad i,j = 1,2,3 \tag{13}$$

where primes denote derivative with respect to x_3. These expressions yield the following sub-matrices

$$\mathbf{K}^{s_l} = \frac{G_s A_p}{15 L_e} \begin{bmatrix} 31 & -32 & 1 \\ -L_e & 2L_e & -L_e \\ -32 & 64 & -32 \\ 1 & -32 & 31 \\ L_e & -2L_e & L_e \end{bmatrix} \tag{14}$$

and

$$\mathbf{K}^{s_a} = \frac{E_s A_p}{3 L_e} \begin{bmatrix} 7 & -8 & 1 \\ -8 & 16 & -8 \\ 1 & -8 & 7 \end{bmatrix} \tag{15}$$

Similarly, mass element sub-matrices can be obtained as

$$\begin{aligned} m_{ij}^{s_l} = \int_{L_e} \varphi_i \cdot \overline{m}^s \cdot \phi_j \, \mathrm{d}x_3 \, ; \quad & i = 1,2,3,4,5 \, ; \\ & j = 1,2,3 \end{aligned} \tag{16}$$

and

$$m_{ij}^{s_a} = \int_{L_e} \phi_i \cdot \overline{m}^s \cdot \phi_j \, \mathrm{d}x_3 \, ; \quad i,j = 1,2,3 \tag{17}$$

yielding

$$\mathbf{M}^{s_l} = \overline{m}^s L_e \begin{bmatrix} \frac{23}{140} & \frac{11}{105} & \frac{-1}{28} \\ \frac{L_e}{84} & \frac{L_e}{105} & \frac{-L_e}{210} \\ \frac{4}{105} & \frac{16}{35} & \frac{4}{105} \\ \frac{-1}{28} & \frac{11}{105} & \frac{23}{140} \\ \frac{L_e}{210} & \frac{-L_e}{105} & \frac{-L_e}{84} \end{bmatrix} \tag{18}$$

and

$$\mathbf{M}^{s_a} = \frac{\overline{m}^s L_e}{30} \begin{bmatrix} 4 & 2 & -1 \\ 2 & 16 & 2 \\ -1 & 2 & 4 \end{bmatrix} \tag{19}$$

where $\overline{m}^s = \rho_s \pi d/4$ is the distributed mass of the soil column.

2.4 Model of the soil-pile interface

Unlike the formulation of the former model [21], in this new model the relative displacements between pile and soil load-line $\mathbf{u}^p - \mathbf{u}^{s_{\text{int}}}$ are related to the pile-soil contact interaction distributed forces (see Figure 5). Therefore, for an infinitesimal section at a certain depth x_3, one can write:

$$k_l \left(u_i^p - u_i^{s_{\text{int}}}\right) = q_i^p; \quad i = 1, 2 \tag{20a}$$

$$k_a \left(u_3^p - u_3^{s_{\text{int}}}\right) = q_3^p \tag{20b}$$

where $k_l = k_l(\chi, G_{\text{dz}}/G_s)$ and $k_a = k_a(\chi, G_{\text{dz}}/G_s)$ are the lateral and axial distributed impedances, respectively, that represent the stiffness and damping properties of the degraded pile-soil interface. In both cases, material damping is introduced assuming a frequency-independent hysteretic damping model through complex valued coefficients of the form $k_{(\cdot)} = \text{Re}[k_{(\cdot)}](1 + 2\text{i}\xi_{\text{dz}})$, where ξ_{dz} is the soil-pile contact damping coefficient. These distributed impedances can be written as

$$k_l(\chi, G_{\text{dz}}/G_s) = F_l(\chi, G_{\text{dz}}/G_s) \cdot E_s \tag{21a}$$

$$k_a(\chi, G_{\text{dz}}/G_s) = F_a(\chi, G_{\text{dz}}/G_s) \cdot G_s \tag{21b}$$

where $F_l(\chi, G_{\text{dz}}/G_s)$ and $F_a(\chi, G_{\text{dz}}/G_s)$ are proportionality functions that determine the strength of the bond between the pile and the soil. Taking into account that both the diameter and the shear modulus of the degraded zone will, in general, be functions of depth ($\chi = \chi(x_3)$ and $G_{\text{dz}} = G_{\text{dz}}(x_3)$), the distributed impedances and the proportionality functions will, in turn, be also x_3-dependent. Possible distributions of these $F_l(x_3)$ and $F_a(x_3)$ functions are shown in Figure 7. Usually, deficient contact effects will be concentrated close to the ground surface, which is represented by lower values of the proportionality functions in that region than in deeper zones. Later, different values of F_l and F_a will be proposed depending on the level of degradation in the damaged pile-soil interface. It is worth noting here that Equation (21) is similar to the one provided by Guin and Banerjee [19]. In that case, however, the proportionality functions appear divided by the pile diameter d, leading to pile diameter dependent functions.

Taking into account the discretization proposed in Section 2.1 for the displacements along pile and soil load-line (Equations (1) and (5)) and the corresponding sets of shape functions (Equations (2) and (3)), element stiffness sub-matrices can be computed by premultiplying Equation (20) by the shape functions in Equation (3) and integrating along each element. Those element stiffness sub-matrices are labelled as $\mathbf{K}_{\text{dz}}^{p_l}$, $\mathbf{K}_{\text{dz}}^{p_a}$, $\mathbf{K}_{\text{dz}}^{s_l}$ and $\mathbf{K}_{\text{dz}}^{s_a}$, where the indices l and a stand for lateral and axial, respectively, and p and s refer to pile and soil load-line. Then, the entries of the element stiffness sub-matrices can be computed as

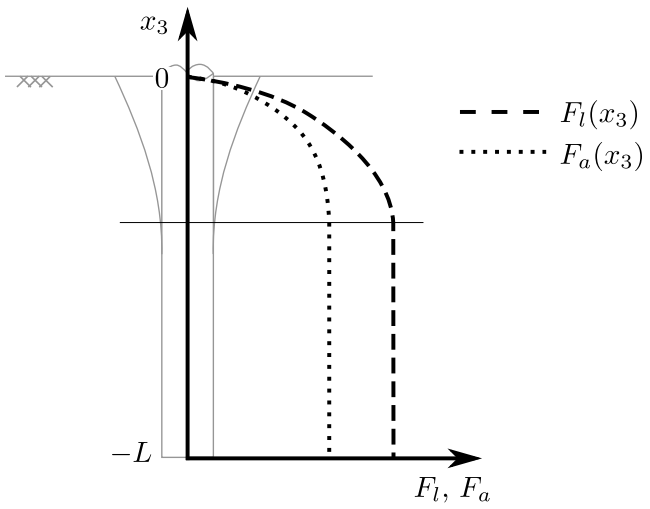

Figure 7: Possible distributions of the F_l and F_a proportionality functions.

$$k^{p_l}_{\mathrm{dz}_{ij}} = \int_{L_e} \phi_i \cdot k_l(x_3) \cdot \varphi_j \,\mathrm{d}x_3\,; \quad i = 1,2,3\,; \quad j = 1,2,3,4,5 \tag{22}$$

$$k^{s_l}_{\mathrm{dz}_{ij}} = \int_{L_e} \phi_i \cdot k_l(x_3) \cdot \phi_j \,\mathrm{d}x_3\,; \quad i,j = 1,2,3 \tag{23}$$

$$k^{p_a}_{\mathrm{dz}_{ij}} = k^{s_a}_{\mathrm{dz}_{ij}} = \int_{L_e} \phi_i \cdot k_a(x_3) \cdot \phi_j \,\mathrm{d}x_3\,; \quad i,j = 1,2,3 \tag{24}$$

For reference, if F_l and F_a are assumed to be constant over the element length, and hence independent of x_3, the degraded zone element stiffness sub-matrices for the lateral and axial behaviour can be written as

$$\mathbf{K}^{p_l}_{\mathrm{dz}} = \frac{L_e K_l}{2} \begin{bmatrix} \frac{23}{70} & \frac{L_e}{42} & \frac{8}{105} & \frac{-1}{14} & \frac{L_e}{105} \\ \frac{22}{105} & \frac{2L_e}{105} & \frac{32}{35} & \frac{22}{105} & \frac{-2L_e}{105} \\ \frac{-1}{14} & \frac{-L_e}{105} & \frac{8}{105} & \frac{23}{70} & \frac{-L_e}{42} \end{bmatrix} \tag{25}$$

$$\mathbf{K}^{s_l}_{\mathrm{dz}} = \frac{L_e K_l}{30} \begin{bmatrix} 4 & 2 & -1 \\ 2 & 16 & 2 \\ -1 & 2 & 4 \end{bmatrix} \tag{26}$$

$$\mathbf{K}^{p_a}_{\mathrm{dz}} = \mathbf{K}^{s_a}_{\mathrm{dz}} = \frac{L_e K_a}{30} \begin{bmatrix} 4 & 2 & -1 \\ 2 & 16 & 2 \\ -1 & 2 & 4 \end{bmatrix} \tag{27}$$

However, as $F_l(x_3)$ and $F_a(x_3)$ will usually vary with depth, these matrices will, in general, be evaluated numerically for each specific case.

Similarly, the entries of the element sub-matrices $\mathbf{Q}^l_{\mathrm{dz}}$ and $\mathbf{Q}^a_{\mathrm{dz}}$ that transforms tractions along the soil load-line to equivalent nodal forces, are computed as

$$q^l_{\mathrm{dz}_{ij}} = q^a_{\mathrm{dz}_{ij}} = \int_{L_e} \phi_i \phi_j \, \mathrm{d}x_3 \, ; \quad i,j = 1,2,3 \tag{28}$$

leading to the following terms

$$\mathbf{Q}^l_{\mathrm{dz}} = \mathbf{Q}^a_{\mathrm{dz}} = \frac{L_e}{30} \begin{bmatrix} 4 & 2 & -1 \\ 2 & 16 & 2 \\ -1 & 2 & 4 \end{bmatrix} \tag{29}$$

Finally, after the assembly of the global matrices, Equation (20) can be expressed in matrix form as

$$\mathbf{K}^p_{\mathrm{dz}} \mathbf{u}^p - \mathbf{K}^s_{\mathrm{dz}} \mathbf{u}^{s_{\mathrm{int}}} = \mathbf{Q}_{\mathrm{dz}} \mathbf{q}^p \tag{30}$$

where $\mathbf{K}^p_{\mathrm{dz}}$ and $\mathbf{K}^s_{\mathrm{dz}}$ are the resulting global stiffness complex matrices for the degraded zone.

2.5 Assembly of the global system matrix of equations

Grouping Equations (9), (10), (11) and (30), assuming compatibility conditions between strata interfaces and equilibrium along the pile-soil interface ($\mathbf{q}^s = -\mathbf{q}^p$), and considering that acting forces at the top of the pile ($\mathbf{F}_{\mathrm{top}}$) are known together with the tractions at the free surface (usually $\mathbf{p}^s = 0$), the dynamic behaviour of the soil-pile foundation system with a degraded soil zone surrounding the pile is defined by the following system matrix of equations:

$$\begin{bmatrix} \mathbf{H}^{ss} & -\mathbf{G}^{sl} & 0 & 0 \\ \mathbf{H}^{ls} & -\mathbf{G}^{ll} & 0 & \mathbf{C} \\ 0 & \mathbf{Q} & (\mathbf{K}^p - \omega^2 \mathbf{M}^p) & -(\mathbf{K}^s - \omega^2 \mathbf{M}^s) \\ 0 & -\mathbf{Q}_{\mathrm{dz}} & -\mathbf{K}^p_{\mathrm{dz}} & \mathbf{K}^s_{\mathrm{dz}} \end{bmatrix} \begin{bmatrix} \mathbf{u}^s \\ \mathbf{q}^s \\ \mathbf{u}^p \\ \mathbf{u}^{s_{\mathrm{int}}} \end{bmatrix} = \begin{bmatrix} \mathbf{G}^{ss} \mathbf{p}^s \\ \mathbf{G}^{ls} \mathbf{p}^s \\ \mathbf{F}_{\mathrm{top}} \\ 0 \end{bmatrix} \tag{31}$$

Equation (31) converges to that provided by Padrón et al. [21] when k_l, $k_a \to \infty$, situation in which $\mathbf{u}^{s_{\mathrm{int}}} = \mathbf{u}^p$.

3 Results

The object of this section is twofold: (i) to verify that the proposed simplified coupled BEM-FEM model can really be used to study the problem initially described of lateral vibration of a pile with degraded pile-soil interface, and (ii) to calibrate the proportionality function $F_l(\chi, G_{\mathrm{dz}}/G_s)$ for such a problem.

To do so, results obtained with the BEM-FEM model proposed herein are going to be compared against the ones obtained from a more rigorous three-dimensional multi-domain BEM approach for three different configurations.

The first configuration is characterized by a degraded zone with constant diameter, extending along the whole pile and with $\xi_{\mathrm{dz}} = 0$ (see Figure 8a), and will serve the purpose of obtaining an expression for function $F_l(\chi, G_{\mathrm{dz}}/G_s)$. The second configuration will incorporate material damping

in the degraded zone as a function of damage (see Figure 8b), and will be useful to calibrate the damping parameter of the pile-soil interface in the simplified model. Finally, the third configuration will be less simplified, with an inverted truncated conical damaged zone only along the upper part of the pile (see Figure 8c), and will show that the proposed model and proportionality function is adequate to reproduce also more complex configurations such as this one.

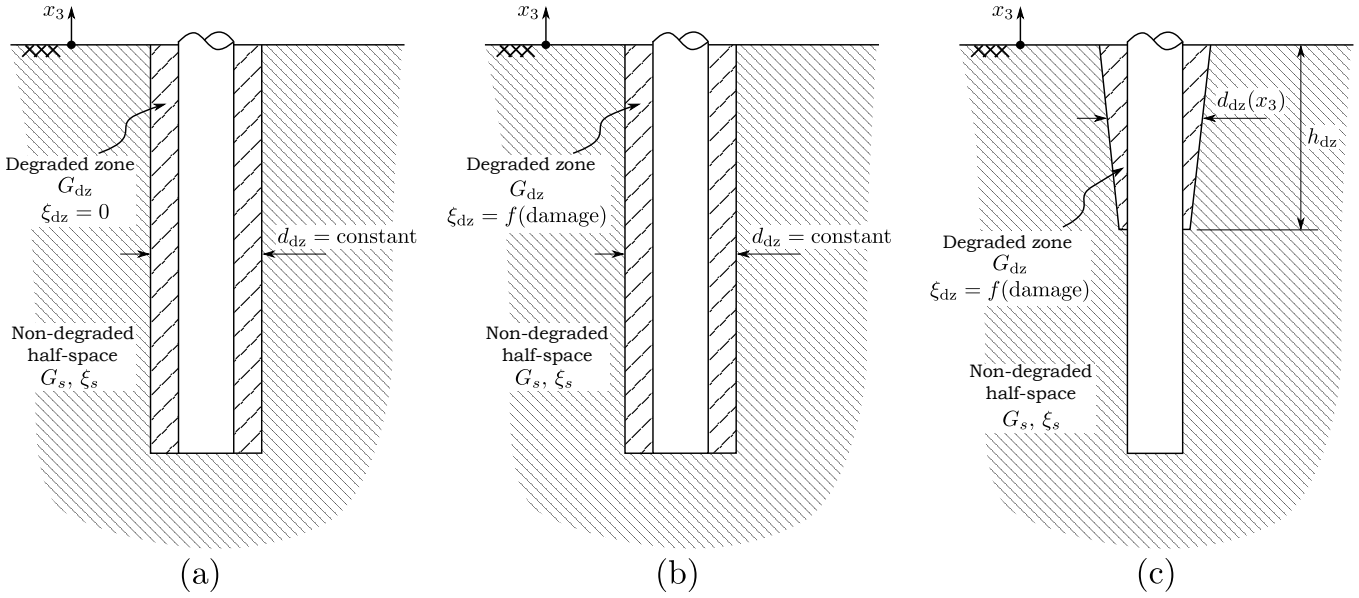

Figure 8: (a) First configuration analysed, with a degraded zone of constant diameter along the whole length of the pile ($\xi_{\mathrm{dz}} = 0$). (b) Second configuration analysed, with a degraded zone of constant diameter along the whole length of the pile and taking the damping in the degraded domain into account ($\xi_{\mathrm{dz}} = f(\text{damage})$). (c) Third configuration analysed, with an inverted truncated conical degraded zone.

3.1 Multi-domain BEM reference model

The multi-domain BEM model taken as reference for verification and calibration of the coupled BEM-FEM model developed here, is the one developed and implemented by Maeso et al. [15]. Through this model, a rigorous continuum mechanics solution of the problem is obtained. A linear system of equations is derived from the singular boundary integral equation for elastodynamics [57]. This way, the unknown boundary displacements and tractions are obtained.

Each of the domains that constitute the soil-foundation system, i.e. pile, half-space and degraded zone, are governed by the integral equation

$$\mathbf{c}^{\iota}\mathbf{u}^{\iota} + \int_{\Gamma^m} \mathbf{p}^{*}\mathbf{u}\,\mathrm{d}\Gamma = \int_{\Gamma^m} \mathbf{u}^{*}\mathbf{p}\,\mathrm{d}\Gamma \tag{32}$$

corresponding to a continuum, finite or semi-infinite, isotropic, homogeneous, linear, viscoelastic medium. All boundaries are discretized into quadratic elements of triangular and quadrilateral shapes with six and nine nodes, respectively. Then, for each region Ω_m, Equation (32) can be written in all nodes on Γ_m in order to obtain a matrix equation of the type

$$\mathbf{H}^{ss}\mathbf{u}^{s} = \mathbf{G}^{ss}\mathbf{p}^{s} \tag{33}$$

The application of boundary conditions and compatibility between the different domains allows to write the final matrix system of equation that represents the dynamic response of the problem.

Hence, three domains are build and meshed for each configuration: one corresponding to the soil half-space (G_s, ν_s, ρ_s and ξ_s), one corresponding to the pile (E_p, ν_p and ρ_p), and the degraded zone domain (G_{dz}, ν_{dz}, ρ_{dz} and ξ_{dz}). In this case, welded contact conditions are assumed along the interfaces.

3.2 Calibration of proportionality function $F_l(\chi, G_{\mathbf{dz}}/G_s)$

Figure 8a illustrates the first configuration of the study, characterized by a degraded zone of constant diameter and extending along the whole length of the pile, which is embedded in a homogeneous half-space. Three different values are adopted for the ratio between the diameters of degraded zone and pile: $\chi = d_{\mathrm{dz}}/d = 1.2$, 1.4 and 1.6. Another five values are considered for the ratio between the shear modulus of degraded zone and half-space, representing different levels of degradation: $G_{\mathrm{dz}}/G_s = 1.00$, 0.75, 0.50, 0.25 and 0.10.

Two soil types are assumed, stiff and soft, with Young's modulus ratios of $E_p/E_s = 100$ and $E_p/E_s = 1000$, respectively, being E_p the pile Young's modulus. In both soil cases, $\xi_s = 0.01$, $\nu_s = 0.4$, being ν_s the soil Poisson's ratio, and the ratio between densities is $\rho_s/\rho_p = 0.7$. The pile aspect ratio is $L/d = 15$. In this calibration procedure no damping in the degraded zone domain is assumed, but as it is considered to be a crucial aspect, mainly in highly degraded soils, its incorporation to the BEM-FEM formulation is verified below.

Results are presented in terms of horizontal impedance functions normalized by pile diameter and soil Young's modulus. Those impedances are frequency dependent complex functions representing the horizontal resistant force of the foundation when the pile tip is horizontally and harmonically displaced a unit length. In the current formulation: $K_{hh} = k_{hh} + \mathrm{i}a_0 c_{hh}$, in which k_{hh} represents the horizontal foundation stiffness and c_{hh} the horizontal foundation damping, being a_0 the dimensionless frequency defined as $a_0 = \omega d/c_s$, where c_s is the soil shear wave velocity of the undisturbed half-space.

Figures 9a and 9b show an example of the kind of meshes generated for the reference multi-domain BEM analyses, being (a) and (b) the complete and a pile top zoom view of the multi-domain BEM mesh for the particular degraded zone diameter ratio of $\chi = d_{\mathrm{dz}}/d = 1.4$. Figure 9c shows a pile top zoom view of the mesh used by the BEM-FEM simulations. It only includes the free surface boundary elements and the pile finite beam elements. To avoid the truncation effects, and after performing convergence analyses, the radius of the circular free-surface meshed in this analysis was equivalent to four times the pile length.

It is important to notice the high reduction not only in the mesh complexity, but also in the quantity of elements and nodes, leading to considerable computing time reductions. Having the same free surface discretization, the multi-domain BEM mesh for the specific case mentioned above is composed by 10730 nodes and 4183 elements, while the BEM-FEM mesh includes only 3866 nodes and 960 elements, which represents a reduction of 61% in the number of nodes and of 77% in the number of elements. Only 10 of the 960 elements and 21 of the 3866 nodes corresponds to the 1D elements of the pile, so this reduction of elements and nodes is due to removing the interfaces between the pile and the degraded zone, and between the degraded zone and the non-degraded half-space.

The impedance functions obtained from the reference multi-domain BEM model for the different cases specified above are shown in continuous lines in Figures 10 and 11 for soft and stiff soils, respectively. The pile foundation system behaves as expected, as χ increases and G_{dz}/G_s decreases the impedance function decreases. It is important to notice that the soil is not degraded when $G_{\mathrm{dz}}/G_s = 1.00$ (black lines) independently of the χ value. To evaluate the variations on the impedance function as soil degrades, the ratios between the impedances provided by the different degradation grades considered, i.e. $G_{\mathrm{dz}}/G_s = 0.75$, 0.50, 0.25 and 0.10, and the non-degraded case, i.e. $G_{\mathrm{dz}}/G_s = 1.00$, can be computed for each χ case, i.e. $\chi = 1.2$, 1.4 and 1.6. In the following, the reduction of the impedance function is quantified in terms of the static stiffness. When the soft soil is considered ($E_p/E_s = 1000$), the static stiffnesses decrease 1.4, 3.7, 9.2 and 20.1% when $\chi = 1.2$ and soil

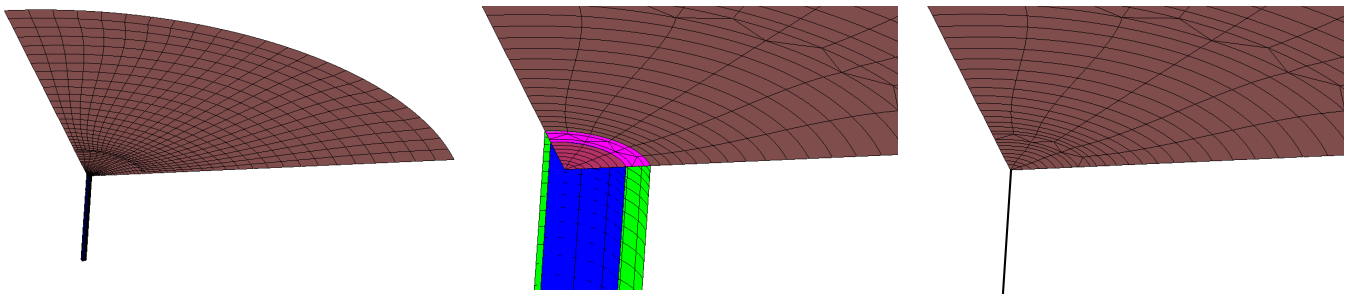

(a) (b) (c)

Figure 9: Complete (a) and top zoom view (b) of a multi-domain BEM mesh for the particular degraded zone diameter ratio of $\chi = d_{\mathrm{dz}}/d = 1.4$, and BEM-FEM mesh detail (c) with 1D elements for the piles. (Only a quarter of the geometry is meshed).

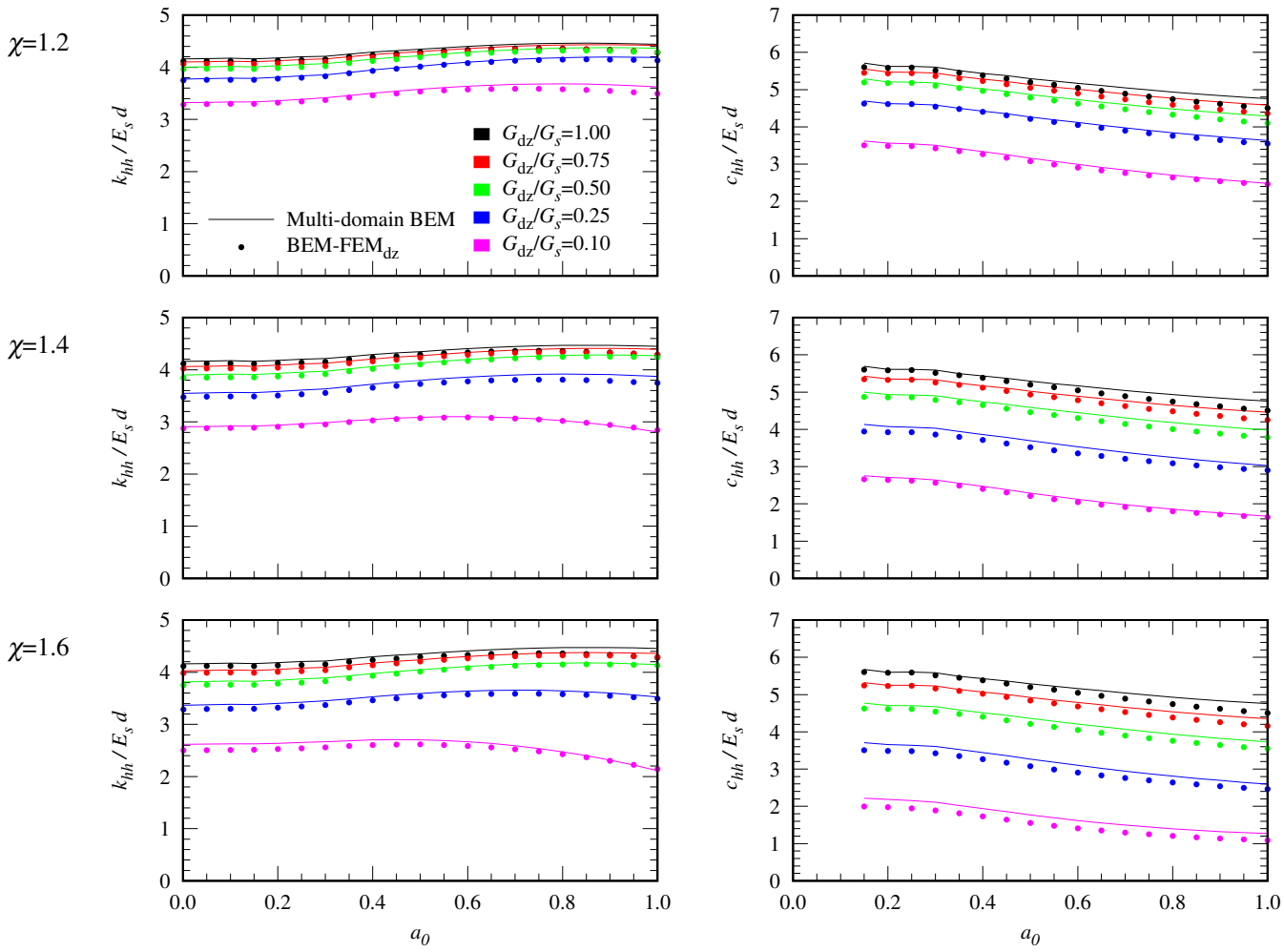

Figure 10: Comparison between stiffness and damping function obtained from the proposed BEM-FEM model and the reference multi-domain BEM model for the case depicted in Figure 8a. $\xi_{\mathrm{dz}} = 0$. $E_p/E_s = 1000$.

degradation is set as $G_{dz}/G_s = 0.75$, 0.50, 0.25 and 0.10, respectively; 2.3, 6.2, 14.7 and 30.1% for $\chi = 1.4$; and 3.2, 8.3, 19.0 and 37.1% for $\chi = 1.6$. Similarly, for the stiff soil cases ($E_p/E_s = 100$), the static stiffnesses decrease 1.8, 5.0, 11.9 and 24.8% when $\chi = 1.2$ and soil degradation is set as $G_{dz}/G_s = 0.75$, 0.50, 0.25 and 0.10, respectively; 3.1, 8.2, 18.6 and 35.8% for $\chi = 1.4$; and 4.2, 10.8, 23.7 and 43.1% for $\chi = 1.6$.

The calibration of the values of the proportionality function F_l for each of the configurations was achieved by performing a sweep of simulations with the simplified BEM-FEM model and finding the values of F_l that minimize the difference between the impedance functions provided by both models. The resulting values of F_l, offering the better matching to the multi-domain BEM simulation results, are summarized in Table 1, and their associated horizontal impedance functions are shown in Figures 10 and 11 for soft and stiff soils, respectively. A very good agreement is found between the impedance functions provided by both models. The dynamic behaviour of the system is reproduced adequately in all the frequency range with a constant value of F_l through all the pile depth.

		G_{dz}/G_s				
		1.00	0.75	0.50	0.25	0.10
χ	1.2	25.0	19.0	13.0	7.0	3.0
	1.4	25.0	16.0	9.0	4.0	1.8
	1.6	25.0	14.0	7.0	3.0	1.2

Table 1: Proposed values of the proportionality function F_l.

The level of agreement does not decrease with soil degradation or frequency, and the proposed model is able to reproduce both the static stiffness and the inertial effects.

As expected, the stiffness and damping of the soil-pile foundation system tend to decrease when the G_{dz}/G_s ratio decreases and also when the size of the degraded zone increases. Another relevant aspect is the low level of dependence of the F_l parameter on the Young's modulus of the pile E_p, the Young's modulus of the soil E_s, and hence, the Young's modulus ratio of the soil-pile foundation system E_p/E_s.

For this reason, a common F_l function for both stiffness ratios is proposed herein as a compromise practical solution in exchange for a small loss in accuracy. Note that this function yields a very slight overestimation of the foundation impedance for $E_p/E_s = 100$ and, on the contrary, a very slight underestimation of the foundation impedance for $E_p/E_s = 1000$. For quantifying this disagreement between the BEM-FEM and the rigorous multi-domain BEM model when considering soft or stiff soil, the mean differences of the static impedance taking into account all χ and G_{dz}/G_s configurations have been computed. The BEM-FEM underestimates the stiffness by only 1.5% when considering $E_p/E_s = 1000$ but overestimates it by 1.7% when considering $E_p/E_s = 100$.

A perfectly bonded behaviour of the pile-soil interface is obtained for $F_l = 25$, used when the soil around the pile is not degraded $G_{dz}/G_s = 1$. The function F_l is also presented in Figure 12 to show qualitatively how it changes with χ and G_{dz}/G_s.

The data presented in Table 1 has been fitted, by the least-squares technique, to the following polynomial function that can be used for interpolation:

$$\begin{aligned} F_l =& 6.114 - 8.560\chi + 258.7\frac{G_{dz}}{G_s} + 3.013\chi^2 - 298.8\chi\frac{G_{dz}}{G_s} - 223.3\left(\frac{G_{dz}}{G_s}\right)^2 + 90.29\chi^2\frac{G_{dz}}{G_s} + \\ &+ 286.0\chi\left(\frac{G_{dz}}{G_s}\right)^2 - 11.23\left(\frac{G_{dz}}{G_s}\right)^3 - 95.40\chi^2\left(\frac{G_{dz}}{G_s}\right)^2 + 27.25\chi\left(\frac{G_{dz}}{G_s}\right)^3 - 9.345\left(\frac{G_{dz}}{G_s}\right)^4 \end{aligned} \tag{34}$$

This expression, whose range of application is for $\chi \in [1.2, 1.6]$ and $G_{dz}/G_s \in [0.10, 1.00]$, is

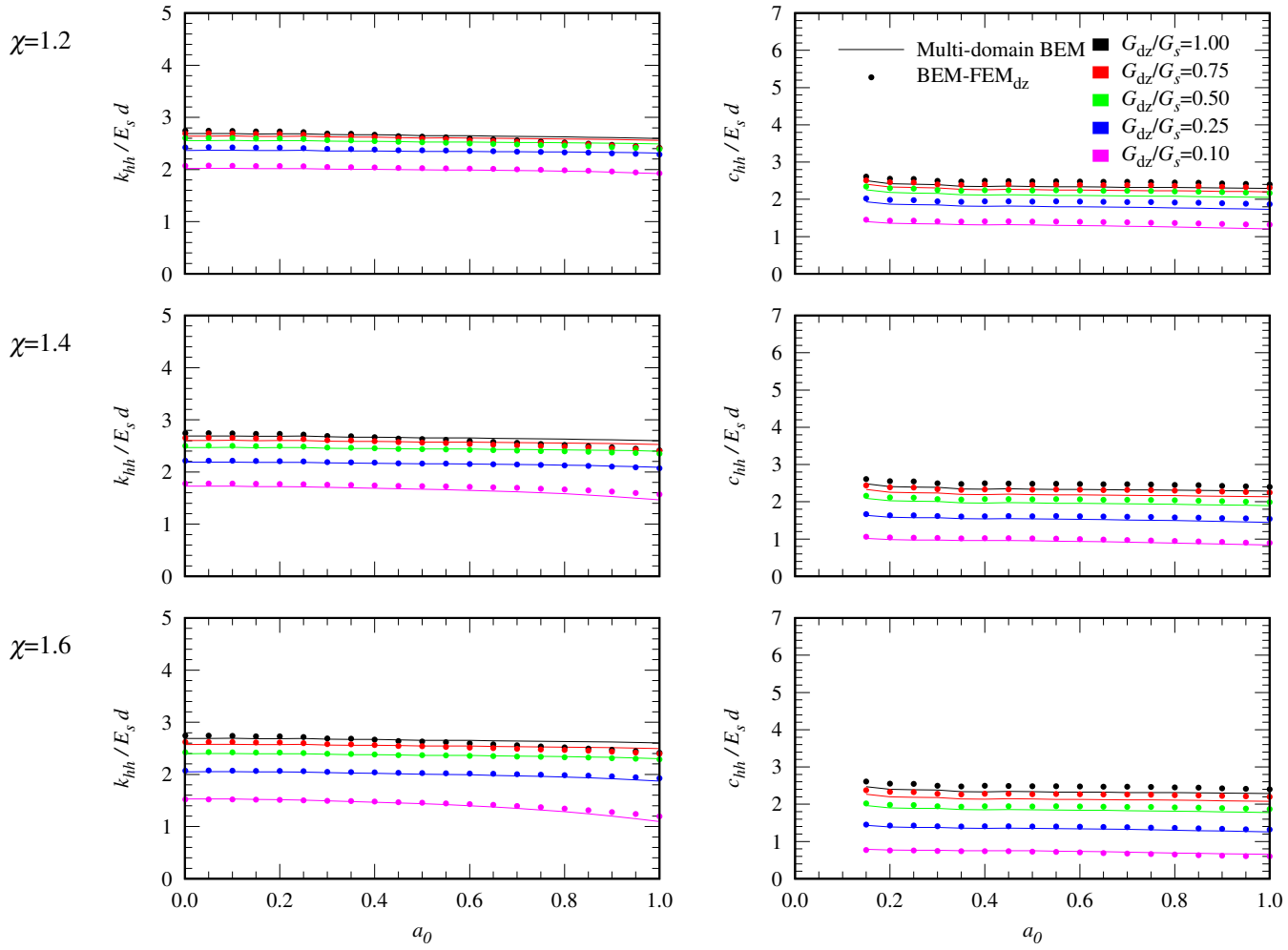

Figure 11: Comparison between stiffness and damping function obtained from the proposed BEM-FEM model and the reference multi-domain BEM model for the case depicted in Figure 8a. $\xi_{\mathrm{dz}} = 0$, $E_p/E_s = 100$.

plotted in Figure 13, where it is shown that it is a smooth surface that contains all the original data present in Table 1 (shown in red points).

3.3 Modelling of material damping in the degraded domain

In the previous section, no material damping was initially considered for the degraded zone. However, and as already mentioned in the introduction, the value of the damping ratio increases significantly with the shear strain and the damage in the soil, and must therefore be adequately incorporated into the model. For highly degraded soils, damping ratios can exceed 20%, which can induce significant variations in the dynamic behaviour of the soil-foundations systems, taking into account that the degraded zone surrounds the vibrating pile.

The expression proposed by Ishibashi and Zang [49] for the degraded soil damping ratios ξ_{dz}, based on experimental tests, is adopted in this section, although other options could also be used. Such expression depends on the plasticity index of the soil I_p and the ratio between the equivalent shear soil modulus and the maximum shear soil modulus $G_{\mathrm{dz}}/G_{\mathrm{max}}$:

$$\xi_{\mathrm{dz}} = \frac{0.333\left(1+e^{-0.0145 I_p^{1.3}}\right)}{2}\left[0.586\left(\frac{G_{\mathrm{dz}}}{G_{\mathrm{max}}}\right)^2 - 1.547\left(\frac{G_{\mathrm{dz}}}{G_{\mathrm{max}}}\right) + 1\right] \tag{35}$$

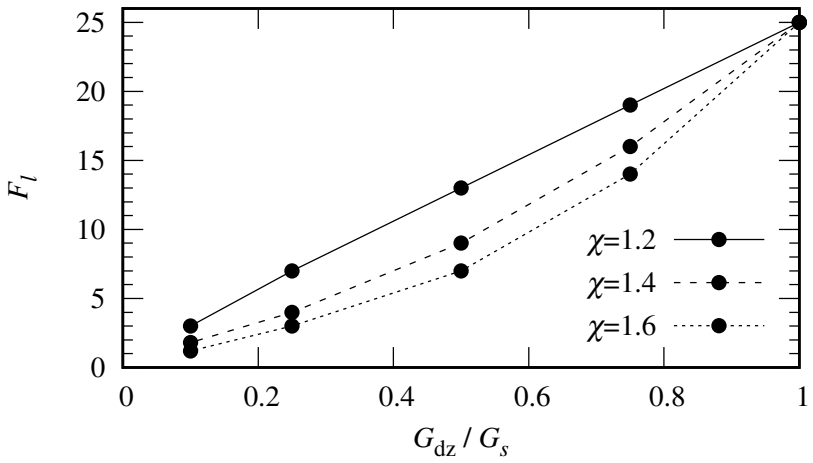

Figure 12: Plot of the proposed proportionality function F_l for the specific values of χ and G_{dz}/G_s studied. Point values shown in Table 1.

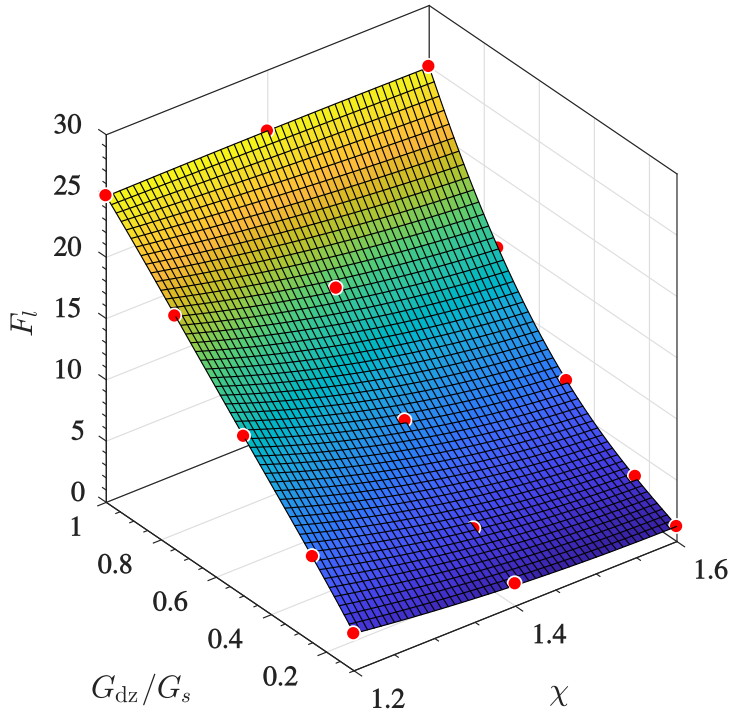

Figure 13: Plot of Equation (34) for the interpolation of the proportionality function F_l. Point values shown in Table 1.

Assuming a medium plasticity index ($I_p = 18.0$) and considering that the maximum shear modulus of the soil is the one of the undisturbed half-space domain ($G_{max} = G_s$), the damping ratios shown in Table 2 are obtained for the different soil degradation levels adopted herein.

Adopting these damping ratios in the definition of the degraded zones for both in the multi-domain BEM and in the proposed BEM-FEM model, the horizontal impedance functions shown in Figure 14 for soft soil and in Figure 15 for stiff soil are obtained. The damping coefficients of the impedance functions strongly change if compared with the ones with $\xi_{dz} = 0$ (Figures 10 and 11 vs. Figures 14 and 15, respectively). Stiffness functions also vary slightly with the inclusion of the degraded zone damping. The good agreement with the results provided by the reference model is maintained. It is demonstrated that the material damping in the degraded domain is perfectly captured by the simpler BEM-FEM model.

G_{dz}/G_s	1.00	0.75	0.50	0.25	0.10
ξ_{dz}	0.010	0.043	0.096	0.166	0.218

Table 2: Damping ratios of the degraded zone based on the expression proposed by Ishibashi and Zang [49] for different levels of degradation.

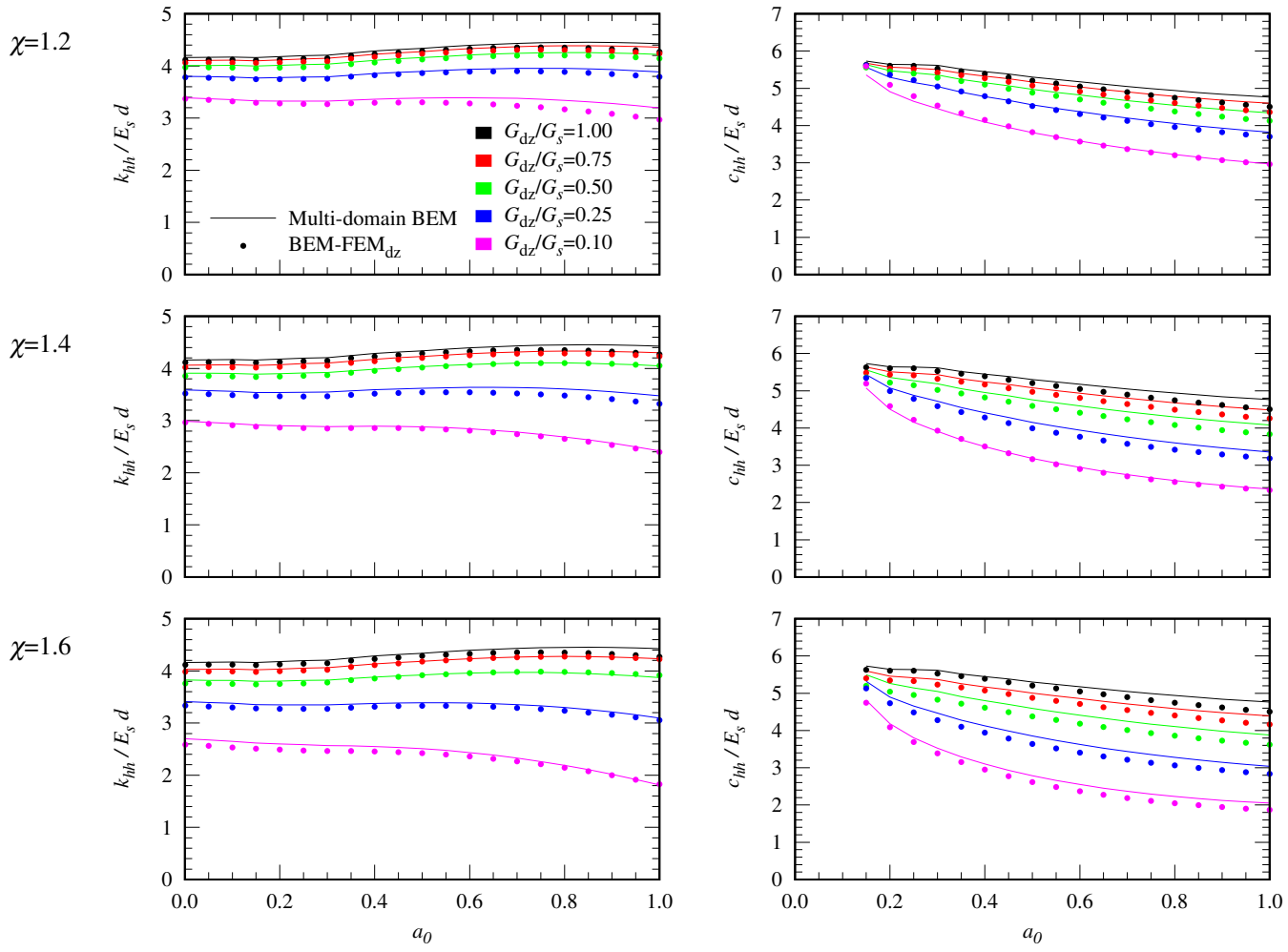

Figure 14: Comparison between stiffness and damping function obtained from the proposed BEM-FEM model and the reference multi-domain BEM model for the case depicted in Figure 8b. $\xi_{dz} \neq 0$, $E_p/E_s = 1000$.

3.4 Verification for a degraded domain with shape changing along pile depth

The utility of the developed tool lies mainly in the possibility of considering a degraded zone whose properties and geometry vary with depth. Usually, the maximum stresses and maximum strains within the soil are located in the surroundings of the piles and close to the surface. Therefore, soil degradation will generally be concentrated in the upper parts of the foundation, and will not be regularly distributed along the pile, as in the first example studied above. Thus, the aim of this subsection is checking whether the proportionality function proposed in the previous section can also be applied to more general configurations.

To do this, the configuration represented in Figure 8c, with an inverted truncated conical degraded zone with $\chi(0) = 1.5$ or 1.6, $\chi(-h_{dz}) = 1.2$, and $h_{dz}/d = 3.0$ and 6.0, is considered in this section, being h_{dz} the depth of the degraded zone. Results are presented in terms of impedance functions for

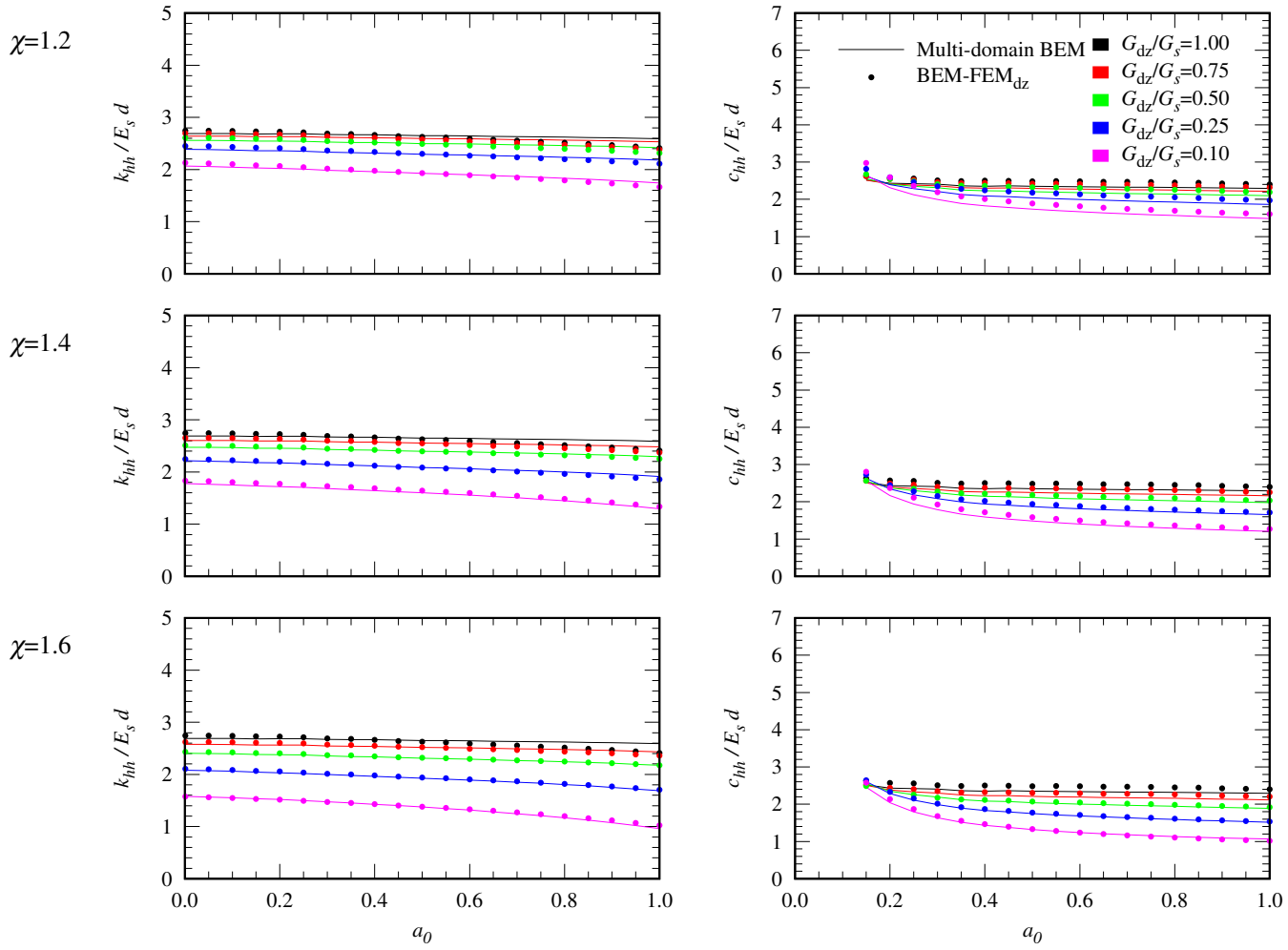

Figure 15: Comparison between stiffness and damping function obtained from the proposed BEM-FEM model and the reference multi-domain BEM model for the case depicted in Figure 8b. $\xi_{dz} \neq 0$, $E_p/E_s = 100$.

$G_{dz}/G_s = 1.00$, 0.75, 0.50, 0.25 and 0.10, as in the previous section. The configurations are studied with both models. In the case of the proposed BEM-FEM formulation, the proportionality functions found in the previous section are implemented, and the degraded zone damping ratio is obtained from Equation (35). On the other hand, Figure 16 shows one of the meshes built for the analyses carried out with the reference multi-domain BEM code.

3.4.1 Verification in terms of impedance functions

For the sake of brevity, only two configurations, are presented here, being the conclusions general to all configurations studied. Impedance functions corresponding to $\chi(0) = 1.6$, $E_p/E_s = 1000$ and $h_{dz}/d = 6.0$ are presented in Figure 17, while impedance functions corresponding to $\chi(0) = 1.5$, $E_p/E_s = 100$, $h_{dz}/d = 3.0$ are presented in Figure 18. It is shown that the proposed model is able to reproduce, with high accuracy, both the stiffness and damping functions provided by the reference multi-domain BEM code, which also means that expression proposed in Equation (34) for the proportionality function F_l can be applied to configurations such as the one studied here.

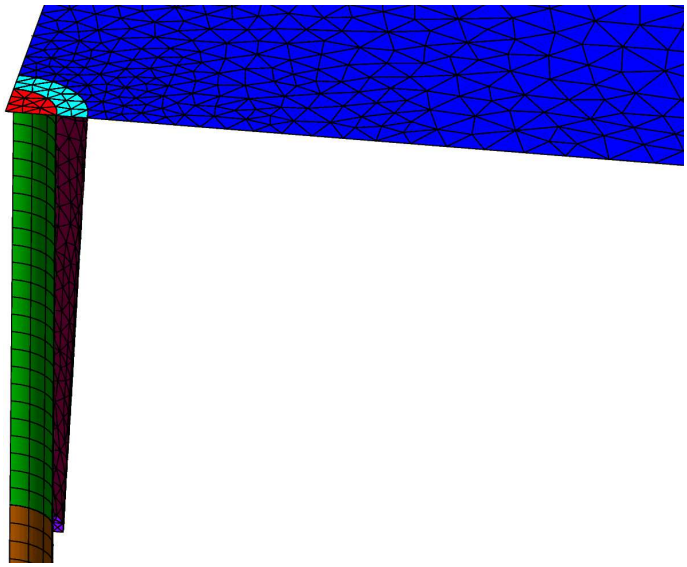

Figure 16: Detail of one of the meshes generated for the multi-domain BEM analyses with the inverted conical degraded zone (only a quarter of the geometry is shown).

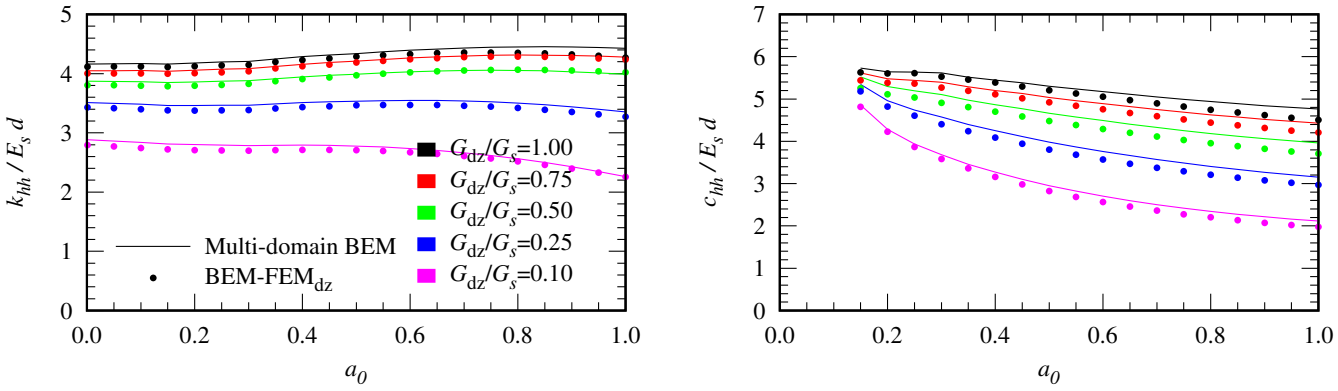

Figure 17: Comparison between stiffness and damping function obtained from the proposed BEM-FEM model and the reference multi-domain BEM model for the case depicted in Figure 8c with an inverted truncated conical degraded zone. $\xi_{\mathrm{dz}} \neq 0$, $E_p/E_s = 1000$, $h_{\mathrm{dz}}/d = 6.0$ and $\chi(0) = 1.6$.

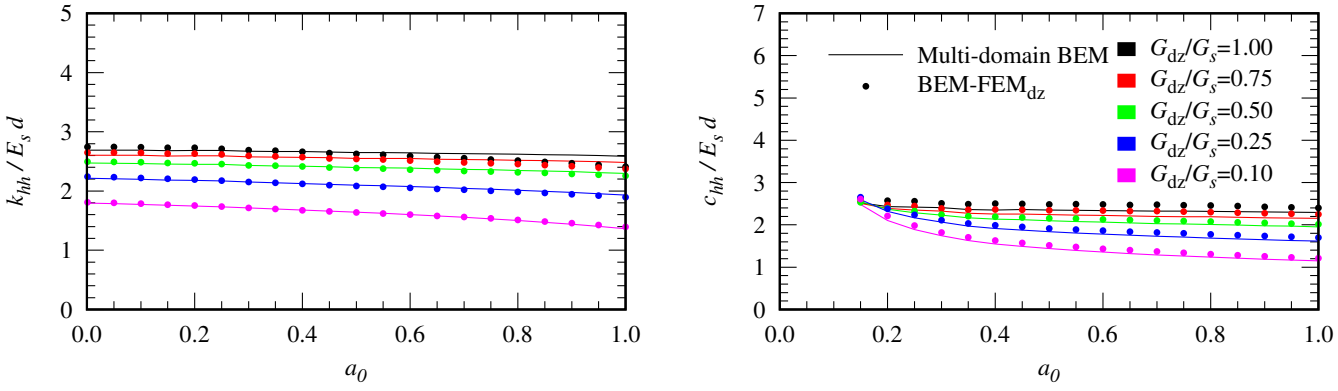

Figure 18: Comparison between stiffness and damping function obtained from the proposed BEM-FEM model and the reference multi-domain BEM model for the case depicted in Figure 8c with an inverted truncated conical degraded zone. $\xi_{\mathrm{dz}} \neq 0$, $E_p/E_s = 100$, $h_{\mathrm{dz}}/d = 3.0$ and $\chi(0) = 1.5$.

3.4.2 Verification in terms of displacements

Apart from these impedance functions, related to the horizontal displacements at pile head, it is also interesting to explore whether the simplified proposed model is also able to reproduce adequately the response of the pile along its length. To this end, Figure 19 presents the distributions of lateral displacements along the pile provided by the proposed BEM-FEM model and the reference multi-domain BEM model for the configuration with $E_p/E_s = 1000$, $\chi(0) = 1.6$ and $h_{\mathrm{dz}}/d = 6.0$. The results are presented for the five relative shear moduli considered for the degraded soil ($G_{\mathrm{dz}}/G_s =$ 1.00, 0.75, 0.50, 0.25 and 0.10) and for three different dimensionless frequencies: $a_0 = 0.0$, 0.5 and 1.0. The figure also displays the displacements obtained for the soil load-line in the coupled BEM-FEM model and the displacements obtained along the interface between degraded zone and non-degraded half-space, in the case of the multi-domain BEM reference model. The deformed shapes are normalized by the pile head displacement, and are plotted taking into account the corresponding shape functions (Equations (2) or (3)).

It can be seen that the agreement between the pile deformed shape obtained from the BEM-FEM model and the reference multi-domain BEM model is very high. It can also be seen that the deformation of the soil load-line follows very accurately that of the degraded zone-half space interface, which means that the term $u^p - u^{s_{\mathrm{int}}}$ is representative of the deformation of the degraded zone.

As expected, the stiffer the degraded zone (from $x_3/d = 0$ to $x_3/d = -h_{\mathrm{dz}}/d = -6$, in this case), the smaller is the separation between pile and soil load-line. Below $x_3/d = -h_{\mathrm{dz}}/d$, were the contact between pile and soil is no longer considered as damaged, the deformed shapes of pile and soil load-line coincide.

4 Conclusions

An equivalent linear model for estimating the dynamic horizontal response of piles considering soil degradation along the soil-pile interface has been presented, implemented and calibrated. Taking as a starting point a previous boundary element-finite element coupled model proposed by some of the authors (Padrón et al. [21]), the formulation proposed herein incorporates the possibility of modelling an imperfect or damaged soil-pile interface along which bounded contact conditions no longer apply. The proportionality functions used to define the distributed springs and dashpots that relate pile and soil displacements have been calibrated for a specific set of configurations by comparison against results of a multi-domain three-dimensional boundary element code. The formulation proposed herein has been shown to be able to reproduce the impedance functions and displacements provided by the more rigorous and computationally costly reference multi-domain BEM model. The proposed coupled BEM-FEM formulation is not only computationally more efficient (it is 7.5 times faster than the multi-domain BEM for the single pile case tackled here) but is also more versatile, and requires much less work in mesh generation. The efficiency of the model will also allow to perform parametric analyses or be incorporated in processes that require a large number of evaluations, such as in many optimization techniques.

The novel aspects of this proposal could easily be integrated into alternative integral numerical approaches, as the main ideas of the model are readily generalizable to other fundamental solutions different from the one used in the paper. For the specific applications shown in the manuscript, the half-space fundamental solution would be more efficient than the full-space used herein. On the other hand, by using the half-space fundamental solution, a loss of generality is obtained because irregular and/or non-horizontal surfaces could not be represented.

The formulation can now be extended to model pile groups, as the boundary element approach used to model the soil allows to take rigorously into account pile-soil-pile interaction effects. It can also be generalized to raked piles. Also, the model can be used to obtain results for sub-structuring analyses, or can incorporate the superstructure or other elements for direct analyses of complete

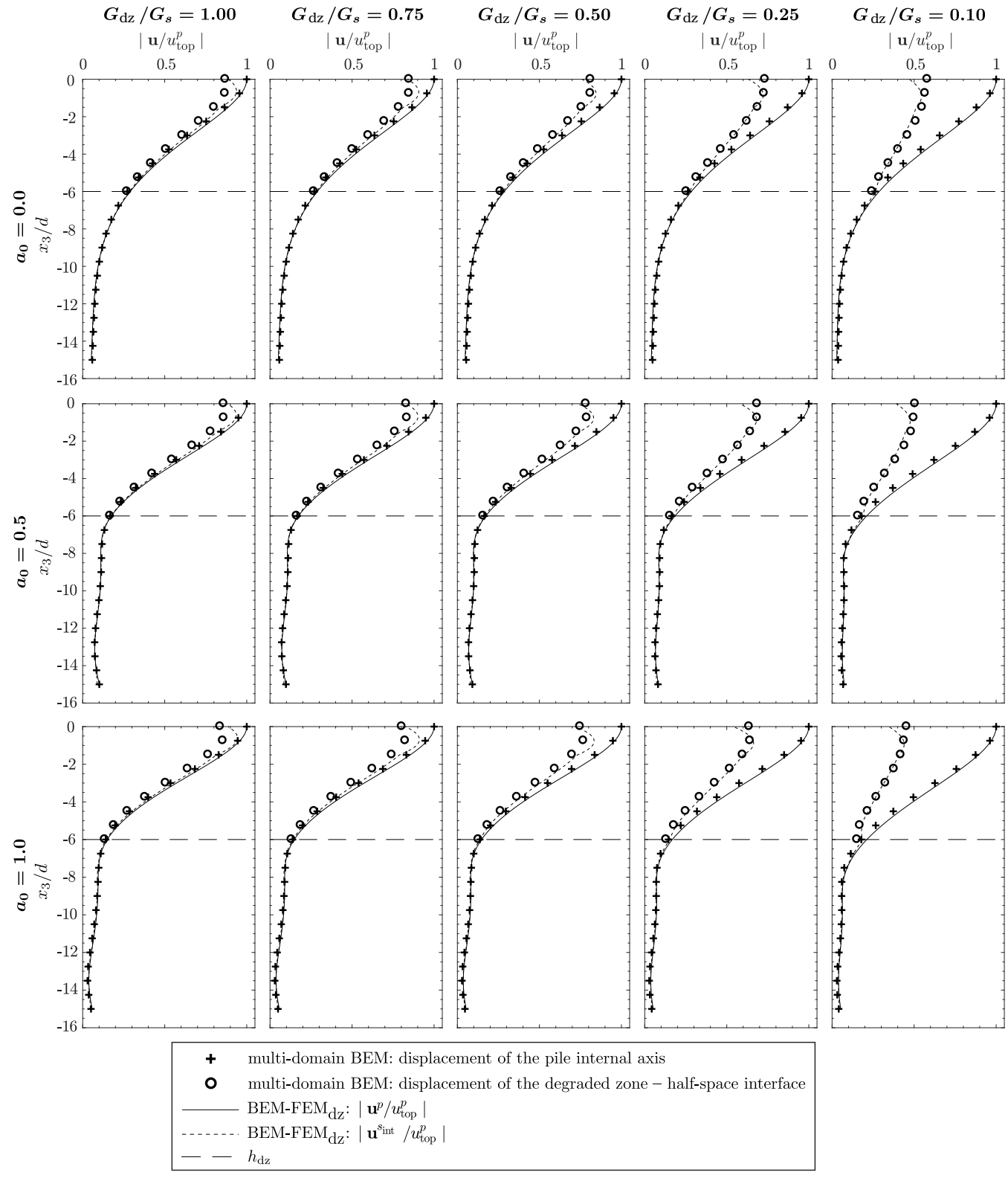

Figure 19: Pile and soil load-line displacements for the case of an inverted truncated conical zone with $E_p/E_s = 1000$, $\chi(0) = 1.6$ and $h_{\mathrm{dz}}/d = 6.0$ and for different degraded zone degradation levels. Comparison between BEM-FEM and reference multi-domain BEM models.

soil-foundation-superstructure systems.

The properties of the pile-soil interface can now be calibrated for different configurations. Here, the comparison against empirical results for specific cases of interest will play a crucial role. At the same time, the definition of those properties of distributed stiffness and damping along the interface could also incorporate more complex models of soil degradation depending for instance on shear strain levels, such as those cited in the introduction of this paper. This updating of the degradation model is intended to be part of future research efforts together with application analyses considering groups of piles, pile inclination, and also stratified soils. In this sense, it would be interesting to analyse how the degradation influences the resonant effects coming from the pile-to-pile interaction, and compare results provided by the model proposed here to the ones existent in the literature, which have been provided either by empirical tests or by using Winkler-based models.

Acknowledgements

This study was supported by the Ministerio de Ciencia, Innovación y Universidades and the Agencia Estatal de Investigación of Spain, and FEDER, through research project BIA2017-88770-R. In addition, F. González is recipient of the FPU fellowship FPU14/06936 from the Ministerio de Ciencia, Innovación y Universidades of Spain. The authors are grateful for this support.

References

[1] R. Y. S. Pak, P. C. Jennings, Elastodynamic response of pile under transverse excitations, Journal of Engineering Mechanics 113 (7) (1987) 1101–1116.

[2] R. K. N. D. Rajapakse, A. H. Shah, On the lateral harmonic motion of an elastic bar embedded in an elastic half-space, International Journal of Solids and Structures 23 (2) (1987) 287–303.

[3] F. Abedzadeh, R. Y. S. Pak, Continuum mechanics of lateral soil-pile interaction, Journal of Engineering Mechanics 130 (11) (2004) 1309–1318.

[4] H. Matlock, L. C. Reese, Generalized solutions for laterally loaded piles, Journal of the Soil Mechanics and Foundations Division 86 (5) (1960) 63–91.

[5] R. Dobry, E. Vicenti, M. J. O'Rourke, J. M. Roesset, Horizontal stiffness and damping of single piles, Journal of the Geotechnical Engineering Division 108 (3) (1982) 439–459.

[6] G. Anoyatis, A. Lemnitzer, Dynamic pile impedances for laterally-loaded piles using improved Tajimi and Winkler formulations, Soil Dynamics and Earthquake Engineering 92 (2017) 279–297.

[7] G. Gazetas, K. Fan, A. Kaynia, E. Kausel, Dynamic interaction factors for floating pile groups, Journal of Geotechnical Engineering 117 (10) (1991) 1531–1548.

[8] F. Dezi, S. Carbonari, G. Leoni, A model for the 3D kinematic interaction analysis of pile groups in layered soils, Earthquake Engineering & Structural Dynamics 38 (11) (2009) 1281–1305.

[9] G. M. Álamo, J. D. R. Bordón, J. J. Aznárez, O. Maeso, Relevance of soil-pile tangential tractions for the estimation of kinematic seismic forces: Formulation and setting of a Winkler approach, Applied Mathematical Modelling 59 (2018) 1–19.

[10] R. L. Kuhlemeyer, Static and dynamic laterally loaded floating piles, Journal of the Geotechnical Engineering Division 105 (2) (1979) 289–304.

[11] A. Velez, G. Gazetas, R. Krishnan, Lateral dynamic response of constrained-head piles, Journal of Geotechnical Engineering 109 (8) (1983) 1063–1081.

[12] C. S. Goit, M. Saitoh, Model tests and numerical analyses on horizontal impedance functions of inclined single piles embedded in cohesionless soil, Earthquake Engineering and Engineering Vibration 12 (1) (2013) 143–154.

[13] S. E. Kattis, D. Polyzos, D. E. Beskos, Vibration isolation by a row of piles using a 3-D frequency domain BEM, International Journal for Numerical Methods in Engineering 46 (5) (1999) 713–728.

[14] S. E. Kattis, D. Polyzos, D. E. Beskos, Modelling of pile wave barriers by effective trenches and their screening effectiveness, Soil Dynamics and Earthquake Engineering 18 (1) (1999) 1–10.

[15] O. Maeso, J. J. Aznárez, F. García, Dynamic impedances of piles and groups of piles in saturated soils, Computers & Structures 83 (10) (2005) 769–782.

[16] R. Sen, T. G. Davies, P. K. Banerjee, Dynamic analysis of piles and pile groups embedded in homogeneous soils, Earthquake Engineering & Structural Dynamics 13 (1) (1985) 53–65.

[17] S. M. Mamoon, A. M. Kaynia, P. K. Banerjee, Frequency domain dynamic analysis of piles and pile groups, Journal of Engineering Mechanics 116 (10) (1990) 2237–2257.

[18] A. M. Kaynia, E. Kausel, Dynamics of piles and pile groups in layered soil media, Soil Dynamics and Earthquake Engineering 10 (8) (1991) 386–401.

[19] J. Guin, P. K. Banerjee, Coupled soil-pile-structure interaction analysis under seismic excitation, Journal of Structural Engineering 124 (4) (1998) 434–444.

[20] Z. Y. Ai, Z. X. Li, Dynamic analysis of a laterally loaded pile in a transversely isotropic multi-layered half-space, Engineering Analysis with Boundary Elements 54 (2015) 68–75.

[21] L. A. Padrón, J. J. Aznárez, O. Maeso, BEM-FEM coupling model for the dynamic analysis of piles and pile groups, Engineering Analysis with Boundary Elements 31 (6) (2007) 473–484.

[22] G. M. Álamo, A. E. Martínez-Castro, L. A. Padrón, J. J. Aznárez, R. Gallego, O. Maeso, Efficient numerical model for the computation of impedance functions of inclined pile groups in layered soils, Engineering Structures 126 (2016) 379–390.

[23] A. Romero, P. Galvín, A BEM-FEM using layered half-space Green's function in time domain for SSI analyses, Engineering Analysis with Boundary Elements 55 (2015) 93–103.

[24] H. El-Marsafawi, Y. C. Han, M. Novak, Dynamic experiments on two pile groups, Journal of Geotechnical Engineering 118 (4) (1992) 576–592.

[25] A. Boominathan, S. Krishna Kumar, R. M. Subramanian, Lateral dynamic response and effect of weakzone on the stiffness of full scale single piles, Indian Geotechnical Journal 43 (1) (2015) 43–50.

[26] S. Biswas, B. Manna, D. K. Baidya, Experimental and theoretical study on the nonlinear response of full-scale single pile under coupled vibrations, Soil Dynamics and Earthquake Engineering 94 (2017) 109–115.

[27] B. El Shamouby, M. Novak, Dynamic experiments with group of piles, Journal of Geotechnical Engineering 110 (6) (1984) 719–737.

[28] B. Manna, D. K. Baidya, Dynamic nonlinear response of pile foundations under vertical vibration – Theory versus experiment, Soil Dynamics and Earthquake Engineering 30 (6) (2010) 456–469.

[29] C. S. Goit, M. Saitoh, Model Tests on Horizontal Impedance Functions of Fixed-Head Inclined Pile Groups under Soil Nonlinearity, Journal of Geotechnical and Geoenvironmental Engineering 140 (6) (2014) 04014023.

[30] Z. Li, S. Escoffier, P. Kotronis, Centrifuge modeling of batter pile foundations under earthquake excitation, Soil Dynamics and Earthquake Engineering 88 (2016) 176–190.

[31] M. N. Hussien, T. Tobita, S. Iai, M. Karray, Soil-pile-structure kinematic and inertial interaction observed in geotechnical centrifuge experiments, Soil Dynamics and Earthquake Engineering 89 (2016) 75–84.

[32] A. Taghavi, K. K. Muraleetharan, G. A. Miller, Nonlinear seismic behavior of pile groups in cement-improved soft clay, Soil Dynamics and Earthquake Engineering 99 (2017) 189–202.

[33] M. H. El Naggar, K. J. Bentley, Dynamic analysis for laterally loaded piles and dynamic p-y curves, Canadian Geotechnical Journal 37 (6) (2000) 1166–1183.

[34] B. K. Maheshwari, H. Watanabe, Nonlinear dynamic behavior of pile foundations: effects of separation at the soil-pile interface, Soils and Foundations 46 (4) (2006) 437–448.

[35] N. Allotey, M. H. El Naggar, A numerical study into lateral cyclic nonlinear soil-pile response, Canadian Geotechnical Journal 45 (9) (2008) 1268–1281.

[36] A. A. Markou, A. M. Kaynia, Nonlinear soil-pile interaction for offshore wind turbines, Wind Energy 21 (7) (2018) 558–574.

[37] A. Rahmani, M. Taiebat, W. D. Liam Finn, C. E. Ventura, Evaluation of p-y springs for nonlinear static and seismic soil-pile interaction analysis under lateral loading, Soil Dynamics and Earthquake Engineering 115 (2018) 438–447.

[38] N. Gerolymos, K. Kassas, E. Bouzoni, R. B. J. Brinkgreve, Dynamic analysis of piles subjected to axial and lateral loading with emphasis on soil and interface nonlinearities, Numerical Methods in Geotechnical Engineering – Proceedings of the 8th European Conference on Numerical Methods in Geotechnical Engineering, NUMGE 2014 2 (2014) 1117–1122.

[39] D. C. Angelides, J. M. Roesset, Non-linear lateral dynamic stiffness of piles, Journal of the Geotechnical Engineering Division 107 (11) (1981) 1443–1460.

[40] K. J. Bentley, M. H. E. Naggar, Numerical analysis of kinematic response of single piles, Canadian Geotechnical Journal 37 (6) (2000) 1368–1382.

[41] D. Bhowmik, D. K. Baidya, S. P. Dasgupta, A numerical and experimental study of hollow steel pile in layered soil subjected to lateral dynamic loading, Soil Dynamics and Earthquake Engineering 53 (2013) 119–129.

[42] M. Novak, M. Sheta, Approximate approach to contact effects of piles, In Proceedings of Session on Dynamic Response of Pile Foundations: Analytical Aspects, ASCE National Convention, Florida (1980) 53–79.

[43] A. S. Veletsos, K. W. Dotson, Impedances of soil layer with disturbed boundary zone, Journal of Geotechnical Engineering 112 (3) (1986) 363–368.

[44] M. Novak, Y. C. Han, Impedances of soil layer with boundary zone, Journal of Geotechnical Engineering 116 (6) (1990) 1008–1014.

[45] Y. C. Han, G. C. W. Sabin, Impedances for radially inhomogeneous viscoelastic soil media, Journal of Engineering Mechanics 121 (9) (1995) 939–947.

[46] C. Luo, X. Yang, C. Zhan, X. Jin, Z. Ding, Nonlinear 3D finite element analysis of soil-pile-structure interaction system subjected to horizontal earthquake excitation, Soil Dynamics and Earthquake Engineering 84 (2016) 145–156.

[47] H. B. Seed, I. M. Idriss, Soil moduli and damping factors for dynamic response analyses. REPORT NO. EERC 70-10, Earthquake Engineering Research Center, University of California, Berkeley, 1970.

[48] M. Vucetic, R. Dobry, Effect of soil plasticity on cyclic response, Journal of Geotechnical Engineering 117 (1) (1991) 89–107.

[49] I. Ishibashi, X. Zhang, Unified dynamic shear moduli and damping ratios of sand and clay, Soils and Foundations 33 (1) (1993) 182–191.

[50] EN1998-5, Eurocode 8 – Design of structures for earthquake resistance. Part 5: foundations, retaining structures and geotechnical aspects, CEN, 2004.

[51] A. V. Mendonça, J. B. Paiva, An elastostatic FEM/BEM analysis of vertically loaded raft and piled raft foundation, Engineering Analysis with Boundary Elements 27 (9) (2003) 919–933.

[52] L. A. Padrón, J. J. Aznárez, O. Maeso, Dynamic analysis of piled foundations in stratified soils by a BEM–FEM model, Soil Dynamics and Earthquake Engineering 28 (5) (2008) 333–346.

[53] L. A. Padrón, J. J. Aznárez, O. Maeso, 3-D boundary element-finite element method for the dynamic analysis of piled buildings, Engineering Analysis with Boundary Elements 35 (3) (2011) 465–477.

[54] L. A. Padrón, J. J. Aznárez, O. Maeso, A. Santana, Dynamic stiffness of deep foundations with inclined piles, Earthquake Engineering & Structural Dynamics 39 (12) (2010) 1343–1367.

[55] T. A. Cruse, F. J. Rizzo, A direct formulation and numerical solution of the general transient elastodynamic problem. I, Journal of Mathematical Analysis and Applications 22 (1) (1968) 244–259.

[56] L. A. Padrón, Numerical model for the dynamic analysis of pile foundations, Doctoral dissertation, Universidad de Las Palmas de Gran Canaria, 2009.

[57] J. Domínguez, Boundary Elements in Dynamics, Computational Mechanics Publications, 1993.